LETTER

https://doi.org/10.1038/s41586-019-1276-2

Group 3 innate lymphoid cells mediate early protective immunity against tuberculosis

Amanda Ardain[1,2,22], Racquel Domingo-Gonzalez[3,22], Shibali Das[3,22], Samuel W. Kazer[4,5,6], Nicole C. Howard[3], Alveera Singh[1,2], Mushtaq Ahmed[3], Shepherd Nhamoyebonde[1,2], Javier Rangel-Moreno[7], Paul Ogongo[1,2,8], Lan Lu[3], Duran Ramsuran[2], Maria de la Luz Garcia-Hernandez[7], Tyler K. Ulland[9], Matthew Darby[10], Eugene Park[9,11], Farina Karim[1], Laura Melocchi[9], Rajhmun Madansein[12], Kaylesh Jay Dullabh[12], Micah Dunlap[3], Nancy Marin-Agudelo[3], Takashi Ebihara[9,11], Thumbi Ndung'u[1,2], Deepak Kaushal[13], Alexander S. Pym[1,2], Jay K. Kolls[14], Adrie Steyn[1,2,15], Joaquín Zúñiga[16,17], William Horsnell[10,18], Wayne M. Yokoyama[9,11,19], Alex K. Shalek[4,5,6], Henrik N. Kløverpris[1,2,20,21], Marco Colonna[7], Alasdair Leslie[1,2,21,23]* & Shabaana A. Khader[3,23]*

Tuberculosis is the leading cause of death by an infectious disease worldwide[1]. However, the involvement of innate lymphoid cells (ILCs) in immune responses to infection with *Mycobacterium tuberculosis* (*Mtb*) is unknown. Here we show that circulating subsets of ILCs are depleted from the blood of participants with pulmonary tuberculosis and restored upon treatment. Tuberculosis increased accumulation of ILC subsets in the human lung, coinciding with a robust transcriptional response to infection, including a role in orchestrating the recruitment of immune subsets. Using mouse models, we show that group 3 ILCs (ILC3s) accumulated rapidly in *Mtb*-infected lungs and coincided with the accumulation of alveolar macrophages. Notably, mice that lacked ILC3s exhibited a reduction in the accumulation of early alveolar macrophages and decreased *Mtb* control. We show that the C-X-C motif chemokine receptor 5 (CXCR5)–C-X-C motif chemokine ligand 13 (CXCL13) axis is involved in *Mtb* control, as infection upregulates CXCR5 on circulating ILC3s and increases plasma levels of its ligand, CXCL13, in humans. Moreover, interleukin-23-dependent expansion of ILC3s in mice and production of interleukin-17 and interleukin-22 were found to be critical inducers of lung CXCL13, early innate immunity and the formation of protective lymphoid follicles within granulomas. Thus, we demonstrate an early protective role for ILC3s in immunity to *Mtb* infection.

ILCs share features with both adaptive and innate immune cells and comprise three main subsets[2,3]. Type 1 ILCs produce interferon (IFN)-γ and include natural killer (NK) cells and non-cytotoxic, non-NK type 1 ILCs[2,3]. Group 2 ILCs, which produce interleukin (IL)-4, IL-5 and IL-13, are involved in inflammatory-linked airway hyperactivity, tissue repair and helminth clearance[2,3]. ILC3s produce IL-17 and/or IL-22[4], and can participate in the strategic positioning of immune cells in ectopic lymphoid structures[5]. Circulating ILC3s are enriched for unipotent and multipotent ILC precursors, and can give rise to all known ILC subsets, including NK cells in vivo[6]. ILCs are crucial for tissue repair of the lungs following infection[7] and for generating hepatic granulomas[8]. Thus, we investigated the role of ILCs in the immune responses to tuberculosis. Using a validated flow cytometry panel (Extended Data Fig. 1), we found that blood ILCs were highly depleted in participants infected with tuberculosis compared to control participants, including the CD117$^+$ ILC3 subset (Fig. 1a), but not NK cells (Extended Data Fig. 2a). ILC depletion was not exacerbated by drug resistance or coinfection with HIV (Fig. 1a and Extended Data Fig. 2b). Using paired samples from participants who were HIV$^-$, we found that ILC1s and ILC3s rebounded after treatment, but ILC2s remained depleted (Fig. 1b). Thus, in contrast to persistent infection with HIV[9], circulating ILC1s and ILC3s were restored once the infection with *Mtb* was cleared, confirming a role for bacteraemia in modulating ILC accumulation. Whether ILC2s recover at a later time point remains to be tested. Depletion of blood ILCs during acute infection with HIV is associated with cell death[9]. However, infection with tuberculosis was not associated with significant changes in caspase-3 expression in ILCs (Extended Data Fig. 2c), but with an increase in the anti-apoptotic marker B cell lymphoma 2 (BCL2) (Fig. 1c). In addition, ILC2s showed a significant upregulation of CD25 (Fig. 1d), a marker of activation and pro-survival phenotype in T cells[10]. These data suggest that circulating ILCs respond to infection with *Mtb* but are not lost from the blood due to cell death.

We next investigated whether ILCs accumulate in the lungs following infection with *Mtb* using a mouse model. C57BL/6 mice infected with aerosolized *Mtb* showed rapid early accumulation of ILC3s, but not ILC1s, with later accumulation of ILC2s (Fig. 2a and Extended Data Fig. 3) and the number of ILC3s increased as infection proceeded (Fig. 2a). Simililarly, an ILC3 subset that expressed RAR-related orphan receptor γ-t (Rorγt)–GFP also accumulated during *Mtb* infection in C57BL/6 mice (Fig. 2b). Notably, accumulation of ILC3s coincided with accumulation of alveolar macrophages, and preceded the accumulation of monocytes and recruited macrophages (Fig. 2c) and *Mtb* control in the lung (Fig. 2d). To confirm these observations in humans, we next examined fresh lung tissue, which was surgically resected from participants infected with tuberculosis and identified tissue-resident ILCs using established markers (Extended Data Figs. 1, 4a). In the lung tissue, in contrast to our findings in the blood, all ILC subsets, including NK-p44$^+$ and NK-p44$^-$ ILC3 subpopulations, but not NK cells, were increased compared to healthy lung tissue margins from

[1]Africa Health Research Institute, Durban, South Africa. [2]School of Laboratory Medicine and Medical Sciences, University of KwaZulu-Natal, Durban, South Africa. [3]Department of Molecular Microbiology, Washington University School of Medicine, St Louis, MO, USA. [4]Institute for Medical Engineering and Science, Department of Chemistry, Koch Institute for Integrative Cancer Research, Massachusetts Institute of Technology, Cambridge, MA, USA. [5]Ragon Institute of MGH, MIT and Harvard, Cambridge, MA, USA. [6]Broad Institute of MIT and Harvard, Cambridge, MA, USA. [7]Division of Allergy, Immmunology and Rheumatology, Department of Medicine, Universtiy of Rochester Medical Center, Rochester, NY, USA. [8]Department of Tropical and Infectious Diseases, Institute of Primate Research, Nairobi, Kenya. [9]Division of Immunobiology, Department of Pathology and Immunology, Washington University School of Medicine, St Louis, MO, USA. [10]IDM, University of Cape Town, Cape Town, South Africa. [11]Howard Hughes Medical Institute, Washington University School of Medicine, St Louis, MO, USA. [12]Department of Cardiothoracic Surgery, Nelson Mandela School of Medicine, University of KwaZulu-Natal, Durban, South Africa. [13]Tulane National Primate Research Center, Covington, LA, USA. [14]Tulane University Health Sciences, New Orleans, LA, USA. [15]Department of Microbiology, Centres for AIDS Research and Free Radical Biology, University of Alabama at Birmingham, Birmingham, AL, USA. [16]Instituto Nacional de Enfermedades Respiratorias Ismael Cosio Villegas, Mexico City, Mexico. [17]Tecnologico de Monterrey, Escuela de Medicina y Ciencias de la Salud, Mexico City, Mexico. [18]Institute of Microbiology and Infection, College of Medical and Dental Sciences, University of Birmingham, Birmingham, UK. [19]Division of Rheumatology, Department of Medicine, Washington University School of Medicine, St Louis, MO, USA. [20]Department of Immunology and Microbiology, University of Copenhagen, Copenhagen, Denmark. [21]Department of Infection and Immunity, University College London, London, UK. [22]These authors contributed equally: Amanda Ardain, Racquel Domingo-Gonzalez, Shibali Das. [23]These authors jointly supervised this work: Alasdair Leslie, Shabaana A. Khader. *e-mail: al.leslie@ahri.org; sakhader@wustl.edu

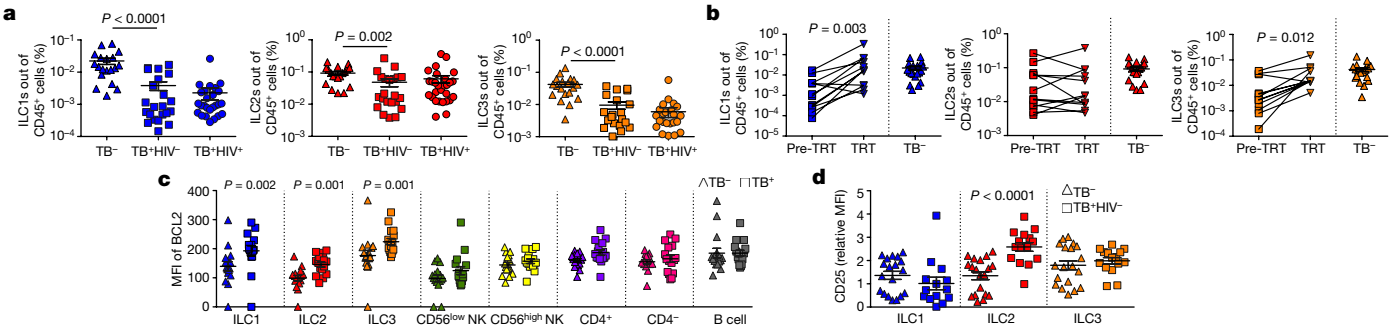

Fig. 1 | Circulating ILCs are depleted and activated in response to tuberculosis. a, Circulating ILC subsets were enumerated in blood of 50 participants with tuberculosis who were HIV$^+$ ($n = 28$) or HIV$^-$ ($n = 22$), and healthy controls ($n = 19$) by flow cytometry. Significance was determined by Kruskal–Wallis test with corrections for multiple comparisons. **b**, Paired ILC subsets in the blood before and after standard tuberculosis treatment ($n = 12$) were compared to frequencies in healthy controls ($n = 19$; P value by Wilcoxon matched-pairs test). Pre-TRT, untreated; TRT, after treatment. **c**, The median fluorescent intensity (MFI) of the anti-apoptotic marker BCL2 was measured in participants who were tuberculosis-positive ($n = 15$–16) and control participants ($n = 16$) on all ILC subsets, and in CD56^{high} NK cells, but not CD56^{low} NK cells, CD4$^+$, CD4$^-$CD3$^+$ T cells and CD19-expressing B cells. Significance was determined by unpaired Mann–Whitney U-test with Bonferroni corrections. **d**, Expression of activation and pro-survival marker CD25 was determined using flow cytometry in ILC subsets in blood from participants with tuberculosis who were HIV$^-$ ($n = 19$). Significance was determined by Kruskal–Wallis test with corrections for multiple comparisons.

lungs of controls who were not infected with tuberculosis (Fig. 2e and Extended Data Fig. 4b, c). Notably, this was not affected by HIV coinfection (Extended Data Fig. 4d). Together, our results show that although circulating ILCs are reduced during pulmonary tuberculosis, they are rapidly increased upon infection in mice and accumulate in the lungs of both *Mtb*-infected mice and human participants who are infected with *Mtb*.

The chemokine CXCL13 is induced in mouse and human lungs during infection with tuberculosis[11] and recruits lymphocytes through CXCR5 to mediate their spatial organization within lymphoid structures called inducible bronchus-associated lymphoid tissues (iBALT)[11]. Consistent with this, high levels of CXCL13 were detected in the plasma of participants with pulmonary tuberculosis, and these were reduced following tuberculosis treatment (Fig. 2f), irrespective of coinfection with HIV (Extended Data Fig. 4e). Furthermore, CXCR5 expression on all human blood ILC subsets was increased (Fig. 2g), and in addition CD103 expression (Extended Data Fig. 4f), a tissue-resident lymphocyte marker, was also increased. Subsequently, we detected distinct

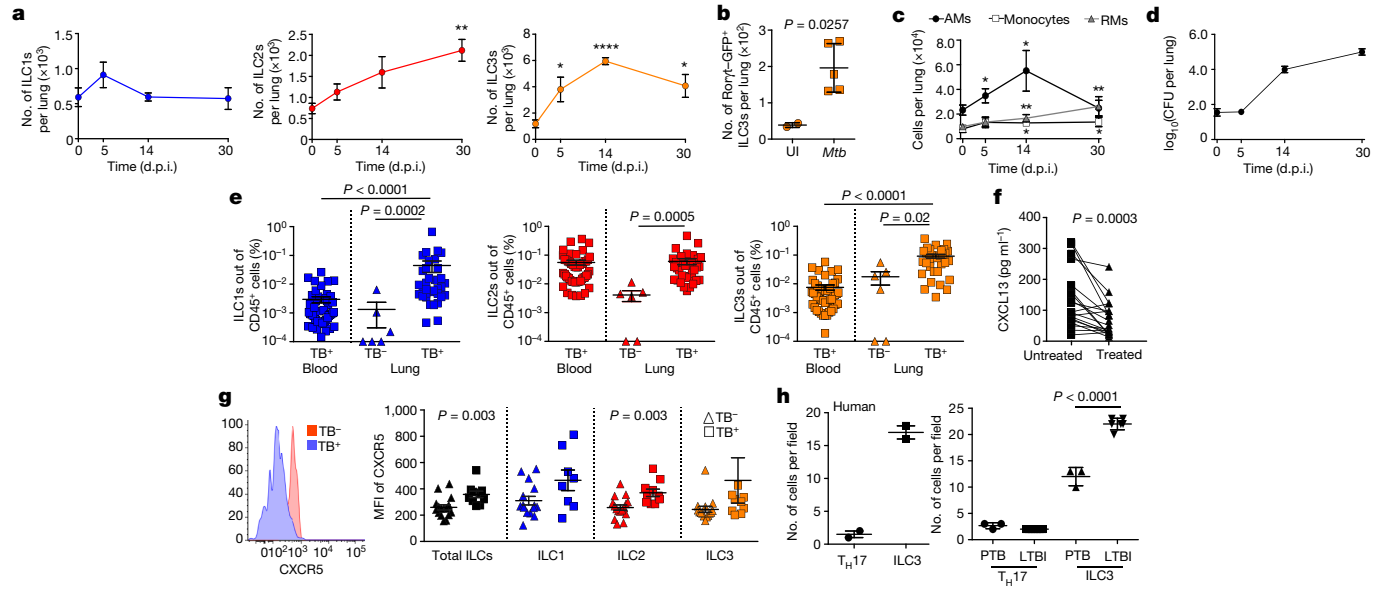

Fig. 2 | ILCs rapidly accumulate within lung tissues and are associated with lymphoid follicle-containing granulomas. a–**c**, C57BL/6 (B6, $n = 5$) mice or Rorγt–GFP ($n = 3$–5) mice were aerosol-infected with around 100 CFU *Mtb*. **a**, Numbers of ILC1s, ILC2s and ILC3s in C57BL/6 mice. **b**, The number of ILC3s in Rorγt–GFP mice were quantified by flow cytometry analyses. **c**, Numbers of alveolar macrophages (AMs), monocytes and recruited macrophages (RMs) were measured and quantified by flow cytometry analyses in C57BL/6 mice ($n = 5$). **d**, Bacterial burden was measured in the lungs of C57BL/6 mice by plating on 7H11 agar plates for 14 days ($n = 5$ mice per time point). Data shown as mean ± s.e.m. (**a**) or mean ± s.d. (**b**–**d**). $^*P < 0.05$, $^{**}P < 0.01$, $^{****}P < 0.0001$. Significance was determined by Student's t-test (**a**–**c**) and all experiments were repeated at least three times. **e**, Human ILC subsets were measured in tuberculosis-infected lung tissue (TB$^+$) compared to tuberculosis-negative (TB$^-$) control lung tissue, and in the circulation using flow cytometry. Significance was determined by Kruskal–Wallis test with adjustments for multiple comparisons. **f**, CXCL13 protein levels were measured in plasma from subjects with drug-susceptible tuberculosis, and after 6 months of standard tuberculosis treatment (two-tailed Wilcoxon matched-pairs test). **g**, CXCR5 expression was measured on circulating ILC subsets using flow cytometry. Significance was determined by Mann–Whitney U-test with correction for multiple comparisons; only P values that were significant after correction are shown. **h**, ILC3 quantification in the formalin-fixed paraffin-embedded lung sections from human, non-human primates (latent tuberculosis and pulmonary tuberculosis) was carried out by staining with CD3, B220 and RORγt and the number of RORγt$^+$CD3$^-$ (ILC3) and RORγt$^+$CD3$^+$ (T_H17) cells were counted and shown. Data shown as mean ± s.d. Significance by Student's t-test (**h**).

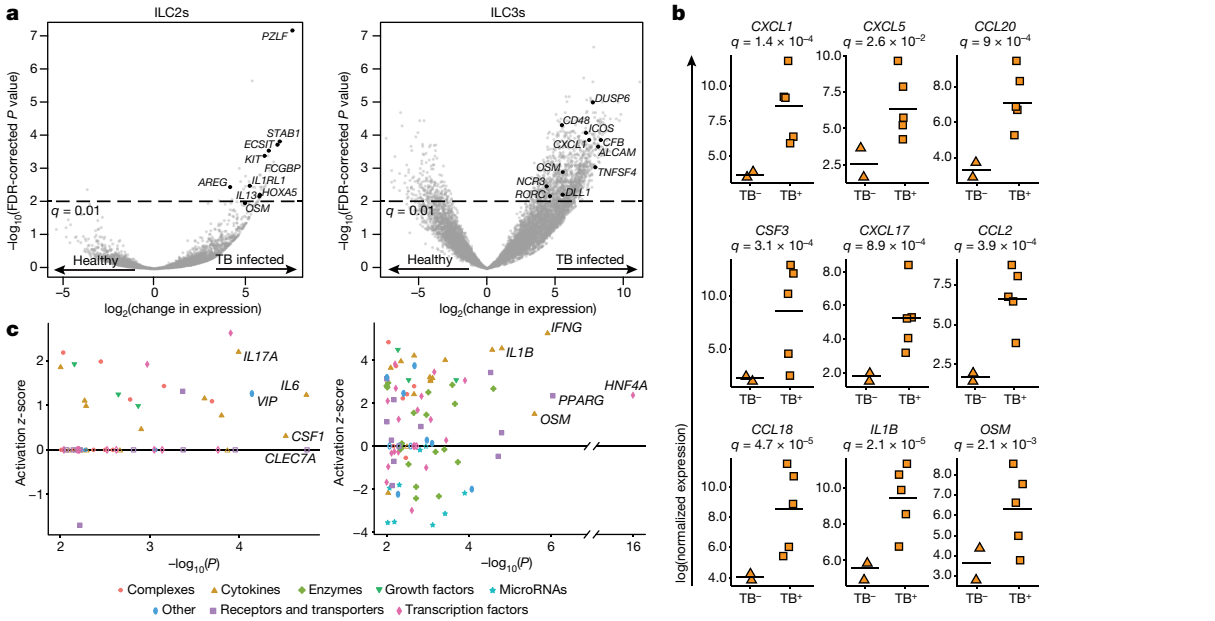

Fig. 3 | ILCs demonstrate a structured response to pulmonary tuberculosis at the transcriptomic level. a, Lung ILC2s and ILC3s were sorted and differential gene expression between tuberculosis-infected ($n = 5$) and uninfected control tissue ($n = 2$) were determined by RNA sequencing. **b**, Expression of key chemokines and chemoattractant proteins significantly upregulated in pulmonary ILCs from participants with tuberculosis (TB^+, $n = 5$) compared to uninfected lungs from control participants is shown (TB^-, $n = 2$). *P* values corrected using Benjamini–Hochberg with a significance cut-off of false-discovery rate (FDR) < 0.01. **c**, Upstream drivers of differentially expressed genes in ILC2s and ILC3s were predicted using ingenuity pathway analysis. *P* values were calculated by hypergeometric test using data from the ingenuity pathway analysis.

populations of CXCR5-expressing ILC3s, and CD103-expressing ILC2s and ILC3s in lung tissue of participants with tuberculosis (Extended Data Fig. 4g). Notably, mouse and human ILCs migrated in response to CXCL13, and this was found to be CXCR5-dependent in mouse ILC3s (Extended Data Fig. 4h, i). Given the role of CXCR5 in iBALT formation, we hypothesized that ILC3s would localize within iBALT-containing tuberculosis lung granulomas. In histological sections from human participants with pulmonary tuberculosis, we confirmed the enrichment of $CD3^-ROR\gamma t^+$ and $CD3^-CD127^+$ ILC3s but not $CD3^+ROR\gamma t^+$ (T helper 17 (T_H17) cells) within granuloma-associated lymphoid follicles compared to the low numbers of $CD3^-ROR\gamma t^+$ ILC3s in necrotic tuberculosis granulomas and non-tuberculosis influenza-infected lung tissue (Fig. 2h and Extended Data Fig. 5a–d). To examine ILC3 localization during tuberculosis latency, we turned to the non-human primate model of *Mtb* infection in macaques[11], where $CD3^-ROR\gamma t^+$ ILC3s localized significantly within the non-necrotic well-formed iBALT-containing tuberculosis granulomas of macaques with latent tuberculosis infections, but not within necrotic granulomas in macaques with pulmonary tuberculosis (Fig. 2h and Extended Data Fig. 5e). These data together show that the CXCL13–CXCR5 axis is involved in functional recruitment of lung ILC3s after infection with *Mtb* and in the localization of ILC3s to iBALT-associated granulomas.

Next, to characterize human lung ILCs, we performed RNA sequencing on ILC2s and ILC3s sorted from fresh resected lungs of participants who were infected with *Mtb* and two controls (sorted based on Extended Data Fig. 1; sort purity shown in Extended Data Fig. 6). Differential expression analysis of ILC2s (45 significant differentially expressed genes) highlighted ILC2 genes that are indicative of inflammatory signalling (*IL13* and *IL1RL1*), tissue repair (amphiregulin (*AREG*)) (Fig. 3a and Supplementary Table 1) and zinc-finger and BTB-domain-containing 16 (*ZBTB16*), which is expressed during ILC development[12]. Notably, ILC2s expressed *KIT*, which is usually associated with ILC3s, but has previously been demonstrated to be expressed in a subset of ILC2s[13]. ILC3s significantly upregulated 1,438 genes (Fig. 3a and Supplementary Table 2), including *RORC* and natural cytotoxic receptor 3 (*NCR3*) and genes encoding pro-inflammatory cytokines (*IL1B*, colony stimulating factor 3 (*CSF3*) and oncostatin M (*OSM*)), which are associated with pulmonary tuberculosis and innate cell recruitment[14,15]. Accordingly, 7 chemokine genes, including *CXCL1* and *CXCL5*, which are central to neutrophil recruitment in pulmonary tuberculosis[16] and the monocyte chemoattractants *CXCL17* and *CCL2* (which encodes sMCP-1) were all upregulated (Fig. 3b). Next, we identified potential upstream regulators of these responses by pathway analysis (Fig. 3c and Supplementary Tables 3, 4). The predicted top upstream drivers of the transcriptional profile that were observed in sorted ILC2s were IL-17, IL-6, CSF-1 and C-type lectin domain family 7 member A (CLEC7A), pathways implicated in pulmonary tuberculosis[17–19], and vasoactive intestinal peptide (VIP), which is known to be elevated during lung inflammation and interacts with the ILC2 marker chemoattractant receptor homologous molecule expressed on T helper type 2 (*CRTH2*)[20]. As VIP had not been directly linked to tuberculosis, we confirmed protein expression in lung tissue from participants with tuberculosis (Extended Data Fig. 7a). Top predicted upstream drivers of ILC3 responses are IFNγ, IL-1β, peroxisome proliferator-activated receptor (PPAR)-γ and hepatocyte nuclear factor (HNF)-4—which have all previously been associated with the tuberculosis immune response[21,22]—and OSM. The latter is less well-studied in tuberculosis infection; however, it is detected in human granuloma[23] and can be seen in the lung tissue sections that were examined in this study (Extended Data Fig. 7b). Construction of gene interaction networks between our differentially expressed genes, and other published gene interactions, suggest that OSM may be linked to other major inflammatory cytokines, and inducers of cell growth and proliferation (Extended Data Fig. 7c and Supplementary Table 5). Moreover, genes downstream of OSM encompassed key immune-response pathways, including IFN signalling, IL-6–STAT and chemotaxis. Lastly, looking across all differentially expressed genes in ILC3s for enriched pathways that describe ILC3 responses (Extended Data Fig. 7d and Supplementary Table 6) highlights IL-17 signalling. Taken together, these transcriptional data from human lung ILCs from participants infected with tuberculosis show a clear response to infection and, in particular, support a role of ILC3s in coordinating lung immunity.

To address the mechanistic role of ILCs during *Mtb* infection, control mice, *Rag1*$^{-/-}$ and *Rag2*$^{-/-}$*Il2rg*$^{-/-}$ double-knockout mice were aerosol-infected with *Mtb* and early immune control was determined

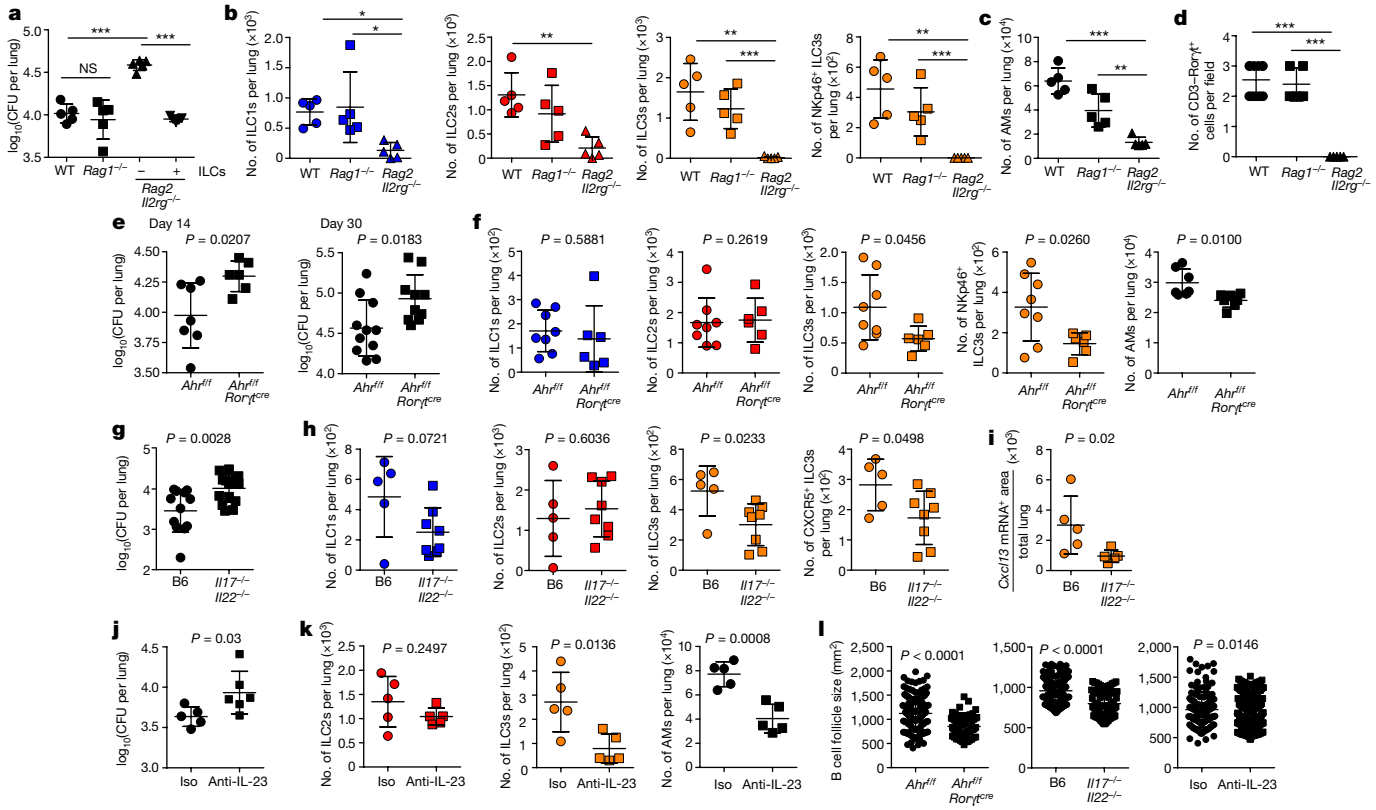

Fig. 4 | ILCs mediate iBALT formation and contribute to early protection from *Mtb*. *Rag1*$^{-/-}$, *Rag2*$^{-/-}$*Il2rg*$^{-/-}$ and wild-type (WT) mice were aerosol-infected with around 100 CFU *Mtb*. ILCs (CD45^{+}CD127^{+}lineage^{-}(Lin^{-})NK1.1^{-}) (Lin: CD3, CD19, CD11c, CD11b, Ter119 and CD5) were isolated from *Mtb*-infected wild-type mice and around 5×10^3 cells were intratracheally transferred into *Rag2*$^{-/-}$*Il2rg*$^{-/-}$ mice 1 day before infection. **a**, Lung bacterial burden at 14 d.p.i. was determined by plating ($n = 5$ per group). NS, not significant. **b**, **c**, Number of ILC1s, ILC2s, total ILC3s and NKp46^{+} ILC3s (**b**) and alveolar macrophages (**c**) were measured by flow cytometry. **d**, ILC3 quantification in histological lung sections was carried out by staining with CD3, B220 and Rorγt and the number of Rorγt^{+}CD3^{-} ILC3s was counted and is shown. **e**, *Ahr*$^{f/f}$ and *Ahr*$^{f/f}$*Rorγt*^{cre} mice were aerosol-infected with around 100 CFU *Mtb* and lung bacterial burden at 14 and 30 d.p.i. was determined by plating ($n = 7$–10 mice per group). **f**, Number of ILC1s, ILC2s, total ILC3s, NKp46^{+} ILC3s and alveolar macrophages were enumerated by flow cytometry. **g**, C57BL/6 and *Il17*$^{-/-}$*Il22*$^{-/-}$ double-knockout mice were aerosol-infected with 100 CFU *Mtb* and lung bacterial CFUs were measured by plating on 7H11 agar plates for 14 days ($n = 12$ per mice per group). **h**, Number of ILC1s, ILC2s, ILC3s, CXCR5^{+} ILC3s, and CXCR5^{+}NKp46^{+} ILC3s were measured by flow cytometry ($n = 5$ C57BL/6 mice, $n = 8$ *Il17*$^{-/-}$*Il22*$^{-/-}$ mice). **i**, Formalin-fixed paraffin-embedded lung sections were subjected to in situ hybridization with the mouse *Cxcl13* probe and the area of *Cxcl13* mRNA^{+} signal per lung over the total lung area was quantified. **j**, **k**, C57BL/6 mice received IL-23 blocking antibody or isotype control antibody (by intraperitoneal injection) 1 day before infection with around 100 CFU *Mtb* and the lung bacterial burden (**j**) and numbers of alveolar macrophages, ILC2s and ILC3s (**k**)were quanified at 14 d.p.i. using plating and flow cytometry, respectively ($n = 5$ mice for isotype, $n = 5$–6 mice for anti-IL-23 antibody). Iso, isotype antibody. **l**, Formalin-fixed paraffin-embedded lung sections from *Mtb*-infected mice at 30 d.p.i. were stained with antibodies against B220 and CD3, and the average sizes of B cell follicles were quantified in *Ahr*$^{f/f}$, *Ahr*$^{f/f}$*Rorγt*^{cre}, C57BL/6, *Il17*$^{-/-}$*Il22*$^{-/-}$ double-knockout, isotype antibody-treated C57BL/6 and anti-IL-23-antibody-treated C57BL/6 *Mtb*-infected mice. All data are mean ± s.d. Significance was determined by either one-way analysis of variance (ANOVA) (**a**–**d**) or Student's *t*-test (**e**–**l**). All experiments were replicated at least twice.

before accumulation of adaptive T cell responses occurred[24]. Whereas *Rag1*$^{-/-}$ mice maintained early innate *Mtb* control similar to wild-type mice at 14 days after infection (d.p.i.), *Rag2*$^{-/-}$*Il2rg*$^{-/-}$ mice exhibited an increase in *Mtb* colony-forming units (CFUs) and this coincided with an absence of all lung ILC subsets (Fig. 4a, b). Notably, increased early *Mtb* CFUs in *Rag2*$^{-/-}$*Il2rg*$^{-/-}$ mice could be rescued by adoptive transfer of sorted lung ILCs from *Mtb*-infected control mice that expressed *Ccr6*, *Rorγt* (also known as *Rorc*) and *Ahr* (Fig. 4a and Extended Data Fig. 8a, b). These results suggest that innate responses in *Rag1*$^{-/-}$ mice are sufficient to mediate early *Mtb* control provided that common-γ chain-dependent ILCs are present. Furthermore, whereas *Ifng*$^{-/-}$ and *Il13*$^{-/-}$ mice maintained *Mtb* control at 14 d.p.i. (Extended Data Fig. 9a), no changes in any ILC subsets were observed (Extended Data Fig. 9b). By contrast, *Rorγt*$^{-/-}$ mice exhibited increased early *Mtb* lung burden (Extended Data Fig. 9c) and this coincided with decreased ILC3 accumulation, without affecting the ILC1 and ILC2 subsets (Extended Data Fig. 9d). These results were further confirmed using mice with specific deletion of ILC3s—that is, *Ahr*$^{f/f}$ *Rorγt*^{cre} mice—that exhibited increased early and late *Mtb* burdens, decreased ILC3 and NK-p46^{+} ILC3 accumulation and decreased alveolar macrophages in the lung, compared to *Ahr*$^{f/f}$ *Mtb*-infected mice (Fig. 4e, f). Accumulation of ILC1 and ILC2 was comparable between *Ahr*$^{f/f}$*Rorγt*^{cre} and *Ahr*$^{f/f}$ *Mtb*-infected mice (Fig. 4f). This was corroborated in *Cbfb*$^{f/f}$*Nkp46*^{cre} (also known as *Cbfb*$^{f/f}$*Ncr1*^{cre}) mice, in which NKp46^{+} cells—including ILC1s, ILC3s and NK cells—are specifically depleted[25], and in which *Mtb* infection led to a marked reduction in the accumulation of the lung ILC subsets compared with *Mtb*-infected *Cbfb*$^{f/f}$ mice; this coincided with reduced accumulation of alveolar macrophages and resulted in increased early and late susceptibility to *Mtb* infection (Extended Data Fig. 9e, f). Complete depletion of NK cells (Extended Data Fig. 10a) did not affect *Mtb* control (Extended Data Fig. 10b). Additionally, baseline characterization of myeloid and lymphocytic populations in lungs of *Cbfb*$^{f/f}$*Nkp46*^{Cre} and *Ahr*$^{f/f}$*Rorγt*^{cre} mice were comparable (Extended Data Figs. 9h, i and 10c, d). Lung ILC3s produce IL-17 and IL-22 in response to IL-23 stimulation[2,26]. Mouse lung cells infected with *Mtb* produced IL-23 (Extended Data Fig. 10e). Moreover, *Mtb*-infected lung cells produced IL-22 and IL-17 when treated with recombinant IL-23 and IL-1β (Extended

Data Fig. 10f). Furthermore, *Il17*$^{-/-}$*Il22*$^{-/-}$ double-knockout mice displayed a significant early increase in lung *Mtb* burden (Fig. 4g), decreased number of lung ILC3s as well as CXCR5^{+} ILC3s, but not ILC1s or ILC2s, and decreased expression of *Cxcl13* mRNA within granulomas (Fig. 4h, i). Accordingly, in vivo early neutralization of IL-23 in C57BL/6 mice resulted in increased early *Mtb* burden (Fig. 4j) and reduced accumulation of early lung ILC3s (Fig. 4k), when compared with isotype-control-treated C57BL/6 mice (Fig. 4j). Notably, these early innate changes resulted in decreased formation of iBALT structures in all models (*Ahr*$^{f/f}$*Ror*γt^{cre}, *Cbfb*$^{f/f}$*Nkp46*^{Cre}, *Il17*$^{-/-}$*Il22*$^{-/-}$ double-knockout mice and IL-23-depleted *Mtb*-infected mice), when compared with their respective controls (Fig. 4l and Extended Data Fig. 9g). Similarly, *Cxcr5*$^{-/-}$ mice also exhibited an increase in lung *Mtb* CFUs and decreased accumulation of ILC3s within lymphoid follicles, as well as decreased formation of iBALT structures (Extended Data Fig. 10g–i). Taken together, these data support an unexpected protective role for ILC3s in regulating early *Mtb* control through the production of IL-17 and IL-22 and formation of iBALT structures in a CXCR5-dependent manner.

Here we show that circulating ILCs are activated and recruited to the lung during infection with tuberculosis in humans. Direct transcriptome sequencing of ILCs from fresh human tissue revealed a coordinated response to infection. These data, therefore, support the participation of ILCs in the human immune response to tuberculosis. Notably, we demonstrate the importance of ILC3s to the outcome of infection using multiple mouse models, showing that a reduction in lung ILC3s impaired early immune control of *Mtb*. The associated increase in lung bacterial burden coincided with decreased IL-17 and IL-22 production, compromised alveolar macrophage accumulation and impaired iBALT organization, which was dependent on the CXCR5–CXCL13 axis—which are key aspects of the immune response to *Mtb*. Taken together, our findings show that ILCs respond to *Mtb* infection and have an important role in determining the outcome of disease during tuberculosis.

Online content

Any methods, additional references, Nature Research reporting summaries, source data, statements of data availability and associated accession codes are available at https://doi.org/10.1038/s41586-019-1276-2.

Received: 2 May 2018; Accepted: 10 May 2019;
Published online: 05 June 2019

1. World Health Organization. *Global Tuberculosis Report 2018*. (2018).
2. Klose, C. S. & Artis, D. Innate lymphoid cells as regulators of immunity, inflammation and tissue homeostasis. *Nat. Immunol.* **17**, 765–774 (2016).
3. Diefenbach, A., Colonna, M. & Koyasu, S. Development, differentiation, and diversity of innate lymphoid cells. *Immunity* **41**, 354–365 (2014).
4. Takatori, H. et al. Lymphoid tissue inducer-like cells are an innate source of IL-17 and IL-22. *J. Exp. Med.* **206**, 35–41 (2009).
5. Jones, G. W. & Jones, S. A. Ectopic lymphoid follicles: inducible centres for generating antigen-specific immune responses within tissues. *Immunology* **147**, 141–151 (2016).
6. Lim, A. I. et al. Systemic human ILC precursors provide a substrate for tissue ILC differentiation. *Cell* **168**, 1086–1100 (2017).
7. Monticelli, L. A. et al. Innate lymphoid cells promote lung-tissue homeostasis after infection with influenza virus. *Nat. Immunol.* **12**, 1045–1054 (2011).
8. Mchedlidze, T. et al. Interleukin-33-dependent innate lymphoid cells mediate hepatic fibrosis. *Immunity* **39**, 357–371 (2013).
9. Kløverpris, H. N. et al. Innate lymphoid cells are depleted irreversibly during acute HIV-1 infection in the absence of viral suppression. *Immunity* **44**, 391–405 (2016).
10. Hedfors, I. A. & Brinchmann, J. E. Long-term proliferation and survival of in vitro-activated T cells is dependent on interleukin-2 receptor signalling but not on the high-affinity IL-2R. *Scand. J. Immunol.* **58**, 522–532 (2003).
11. Slight, S. R. et al. CXCR5^{+} T helper cells mediate protective immunity against tuberculosis. *J. Clin. Invest.* **123**, 712–726 (2013).
12. Constantinides, M. G., McDonald, B. D., Verhoef, P. A. & Bendelac, A. A committed precursor to innate lymphoid cells. *Nature* **508**, 397–401 (2014).
13. Moro, K. et al. Innate production of T_H2 cytokines by adipose tissue-associated c-Kit^{+}Sca-1^{+} lymphoid cells. *Nature* **463**, 540–544 (2010).
14. Dorhoi, A. et al. The adaptor molecule CARD9 is essential for tuberculosis control. *J. Exp. Med.* **207**, 777–792 (2010).
15. Traber, K. E. et al. Induction of STAT3-dependent CXCL5 expression and neutrophil recruitment by oncostatin-M during pneumonia. *Am. J. Respir. Cell Mol. Biol.* **53**, 479–488 (2015).
16. Nouailles, G. et al. CXCL5-secreting pulmonary epithelial cells drive destructive neutrophilic inflammation in tuberculosis. *J. Clin. Invest.* **124**, 1268–1282 (2014).
17. Pagán, A. J. et al. Myeloid growth factors promote resistance to mycobacterial infection by curtailing granuloma necrosis through macrophage replenishment. *Cell Host Microbe* **18**, 15–26 (2015).
18. van de Veerdonk, F. L. et al. Mycobacterium tuberculosis induces IL-17A responses through TLR4 and dectin-1 and is critically dependent on endogenous IL-1. *J. Leukoc. Biol.* **88**, 227–232 (2010).
19. Yadav, M. & Schorey, J. S. The β-glucan receptor dectin-1 functions together with TLR2 to mediate macrophage activation by mycobacteria. *Blood* **108**, 3168–3175 (2006).
20. El-Shazly, A. E. et al. Novel association between vasoactive intestinal peptide and CRTH2 receptor in recruiting eosinophils: a possible biochemical mechanism for allergic eosinophilic inflammation of the airways. *J. Biol. Chem.* **288**, 1374–1384 (2013).
21. Rajaram, M. V. et al. *Mycobacterium tuberculosis* activates human macrophage peroxisome proliferator-activated receptor γ linking mannose receptor recognition to regulation of immune responses. *J. Immunol.* **185**, 929–942 (2010).
22. Tientcheu, L. D. et al. Differential transcriptomic and metabolic profiles of *M. africanum*- and *M. tuberculosis*-infected patients after, but not before, drug treatment. *Genes Immun.* **16**, 347–355 (2015).
23. O'Kane, C. M., Elkington, P. T. & Friedland, J. S. Monocyte-dependent oncostatin M and TNF-α synergize to stimulate unopposed matrix metalloproteinase-1/3 secretion from human lung fibroblasts in tuberculosis. *Eur. J. Immunol.* **38**, 1321–1330 (2008).
24. Khader, S. A. et al. IL-23 and IL-17 in the establishment of protective pulmonary CD4^{+} T cell responses after vaccination and during *Mycobacterium tuberculosis* challenge. *Nat. Immunol.* **8**, 369–377 (2007).
25. Ebihara, T. et al. Runx3 specifies lineage commitment of innate lymphoid cells. *Nat. Immunol.* **16**, 1124–1133 (2015).
26. Cupedo, T. et al. Human fetal lymphoid tissue-inducer cells are interleukin 17-producing precursors to RORC^{+} CD127^{+} natural killer-like cells. *Nat. Immunol.* **10**, 66–74 (2009).

Acknowledgements This work was supported by Washington University in St Louis, NIH grant HL105427, AI111914-02 and AI123780 to S.A.K. and D.K., AI134236-02 to S.A.K., M.C. and D.K., and NIH/NHLBI T32 HL007317-37 to R.D.-G., the Department of Molecular Microbiology, Washington University in St Louis, and Stephen I. Morse Fellowship to S.D., T32 HL 7317-39 to N.C.H. and T32-AI007172 to M. Dunlap. A.L. was supported by BMGF (OPP1137006) and the Wellcome Trust (210662/Z/18/Z), A. Singh and T.N. were supported by the Sub-Saharan African Network for TB/HIV Research Excellence (SANTHE), a DELTAS Africa Initiative (DEL-15-006). J.R.-M. was supported by funds of the Department of Medicine, University of Rochester, and NIH grant U19 AI91036. A.K.S. was supported, in part, by the Searle Scholars Program, the Beckman Young Investigator Program, a Sloan Fellowship in Chemistry, the NIH (5U24AI118672), the Bill and Melinda Gates Foundation and the Ragon Institute. S.W.K. was supported by an NSF Graduate Student Fellowship Award and the Hugh Hampton Young Memorial Fund Fellowship. We thank Amgen for providing the anti-IL-23 antibody for the study, J. Bando for helping with the flow cytometry and M. Holtzman for gifting *Il13*$^{-/-}$ mice.

Reviewer information *Nature* thanks Gérard Eberl, Tom H. M. Ottenhoff and the other anonymous reviewer(s) for their contribution to the peer review of this work.

Author contributions A.A., R.D.-G., S.D., S.W.K., N.C.H., A. Singh, M.A., S.N., J.R.-M., P.O., L.L., D.R., M.d.l.G.-H., T.K.U., M. Darby, E.P., F.K., L.M., R.M., K.J.D., M. Dunlap and N.M.-A. designed, performed and interpreted experiments, T.E., T.N., D.K., A.S.P., J.K.K., A. Steyn, J.Z., W.H., W.M.Y., A.K.S., H.N.K., M.C., A.L. and S.A.K. interpreted experiments, carried out data analysis and/or provided reagents. H.N.K., A.L., M.C. and S.A.K. designed the study, provided funding and wrote the paper, all authors edited and approved the final version of the manuscript.

Competing interests The authors declare no competing interests.

Additional information
Extended data is available for this paper at https://doi.org/10.1038/s41586-019-1276-2.
Supplementary information is available for this paper at https://doi.org/10.1038/s41586-019-1276-2.
Reprints and permissions information is available at http://www.nature.com/reprints.
Correspondence and requests for materials should be addressed to A.L. or S.A.K.
Publisher's note: Springer Nature remains neutral with regard to jurisdictional claims in published maps and institutional affiliations.

METHODS

Data reporting. The experiments were not randomized. The investigators were not blinded to allocation during experiments and outcome assessment unless indicated otherwise.

Participants. Tuberculosis-infected blood and plasma samples were obtained from the collection of urine, blood and sputum (CUBS) cohort, based at the Prince Cyril Zulu Communicable Disease Centre and the Nelson R. Mandela School of Medicine. In total, 50 blood samples were taken from participants with confirmed pulmonary tuberculosis (Gene Xpert, sputum smears or culture method), of which 28 were co-infected with HIV and 22 were HIV-negative. Control blood samples ($TB^{-}HIV^{-}$) were collected from the Females Rising through Empowerment, Support and Health (FRESH) cohort from Umlazi, Durban.

Tuberculosis-affected lung tissue samples were obtained from 36 participants undergoing surgical resections due to severe lung complications, including haemoptysis, bronchiectasis, persistent cavitatory disease, shrunken or collapsed lung or drug-resistant infection, at the King Dinuzulu Hospital in Durban, KwaZulu-Natal and Inkosi Albert Luthuli Central Hospital (IALCH) in Durban, KwaZulu-Natal. In addition, 6 tuberculosis-negative control samples with macroscopically normal tissue margins from lung cancer resections or other inflammatory lung diseases from IALCH in Durban, KwaZulu-Natal were included in the study.

For some histological studies, lung sections were obtained from parcipants with tuberculosis from the Tuberculosis Outpatient Clinic at the National Institute of Respiratory Diseases (INER) in Mexico City. Samples were obtained from participants before anti-*Mtb* treatment.

All participants provided informed consent and each study was approved by the respective institutional review boards including the Biomedical Research Ethics Committee of the University of KwaZulu-Natal or INER.

Sample preparation. Blood samples were processed from frozen peripheral blood mononuclear cells (PBMCs) purified using standard Ficoll separation. Samples were thawed in DNase-containing (25 units ml^{-1}) R10 (Sigma-Aldrich) at 37 °C. Cells were rinsed and rested at 37 °C for a minimum of 1 h before undergoing red-blood-cell lysis by 5–10 ml RBC lysis solution (Qiagen) for 20 min at room temperature. Cells were then stained with the appropriate antibody panel described in Flow cytometry.

Blood for plasma isolation was centrifuged at 2,000 r.p.m. for 10 min. The plasma layer was removed, frozen down in 1-ml aliquots and stored at −80 °C until needed. Later these samples were thawed at room temperature and vortexed thoroughly before use.

Lung samples were processed from fresh tissue immediately after surgery. Resected tissues were washed with cold HBSS (Sigma-Aldrich) and dissected into smaller pieces. Tissues were rinsed again and resuspended in 10 ml R10, containing DNase (1 μl ml^{-1}) and collagenase (4 μl ml^{-1}), and disassociated in a GentleMACS dissociator (Miltenyi Biotec). Cells were rested in a shaking incubator at 37 °C for 30 min and then further processed in the GentleMACS dissociator. After further resting (30 min at 37 °C) and washing steps, cells were strained through a 70-μm cell strainer and washed one final time. Cells were lysed using 5–10 ml RBC lysis buffer (Qiagen) and stained for flow cytometry analysis.

***Mtb* infection in mice.** C57BL/6, *Ifng*$^{-/-}$, *Rag1*$^{-/-}$, *Cxcr5*$^{-/-}$, *Rag2*$^{-/-}$*Il2rg*$^{-/-}$, *Rorγt*$^{-/-}$, *Rorγt*^{GFP} mice were obtained from the Jackson Laboratory and bred at Washington University in St Louis. *Il17*$^{-/-}$ and *Il22*$^{-/-}$ mice were crossed at Washington University in St Louis to obtain double knockout mice. *Cbfb*$^{f/f}$, *Cbfb*$^{f/f}$*Nkp46*^{Cre} breeder pairs[25] were from W.M.Y. *Il13*$^{-/-}$ breeder pairs were a gift from M. Holtzman. *Ahr*$^{f/f}$, *Ahr*$^{f/f}$*Rorγt*^{cre} mice were provided by M.C. The *Mtb* W. Beijing strain, HN878, was cultured to mid-log phase in Proskauer Beck medium containing 0.05% Tween-80 and frozen in 1-ml aliquots at −80 °C. Mice were infected with aerosolized around 100 CFU of bacteria using a Glas-Col airborne infection system. Lungs were collected, homogenized and serial dilutions of tissue homogenates were plated on 7H11 plates and the CFU was counted. Anti-IL-23 (Amgen, 16E5, 500 μg per mouse) and mouse IgG1 isotype (500 μg per mouse) were provided by Amgen and intraperitoneally injected into C57BL/6 mice one day before infection. Anti-NK1.1 (PK136, 100 μg per mouse) and mouse IgG2a isotype (100 μg per mouse) were provided by W.M.Y. and intraperitoneally injected on day 0 and every 3 days after infection. Male and female mice between the ages of 6 and 8 weeks were used for all mouse experiments. Sample sizes were chosen following empirical statistical power analysis based on previous published studies. Histological analysis following mouse experiments were subject to blind analysis. All mice were maintained and used in accordance with approved Washington University in St Louis Institutional Animal Care and Use Committee guidelines.

Flow cytometry. ILCs from human blood and lung tissue were identified by a surface stain that included a near-infrared live/dead cell viability cell staining kit (Invitrogen) and the following monoclonal antibodies: CRTH2 (clone BM16, BD Biosciences), CD127 (clone R34.34, Beckman Coulter), CD117 (clone 104D2, BioLegend), CD56 (clone HCD56, BioLegend), CD25 (clone BC96, BioLegend), CD94 (clone HP-3D9, BD Biosciences), CD161 (clone HP-3G10, BioLegend), NK-p44 (clone Z231, Beckman Coulter), CD16 (clone 3G8, BioLegend), CD4 (clone RPA-T4, BD Biosciences) and CD45 (clone HI30, BD Biosciences). Lineage markers CD19 (clone HIB19, BD Biosciences), CD34 (clone 561, BioLegend), CD14 (clone HCD14, BioLegend), CD4 (clone OKT4, BioLegend), TCRαβ (clone IP26, BioLegend), TCRγδ (clone B1, BioLegend), BDCA2 (clone 201A, BioLegend) and FcER1 (clone AER-37 (CRA1), eBioscience). Intracellular stains were done after using a Fix/Perm kit (BD Biosciences) and included CD3 (clone UCHT1, BD Biosciences) or CD3 (clone HIT3A, BD Biosciences).

Modified antibody panels were used to stain for markers of apoptosis or lung homing. These panels consisted of a near-infrared live/dead cell viability cell staining kit (Invitrogen) and the following monoclonal antibodies: CD117 (clone 104D2, Biolegend), CD45 (clone HI30, BD Biosciences), CD161 (clone HP-3G10, BioLegend), CD56 (clone HCD56, BioLegend), CD94 (clone HP3D9, BD Bioscience), CD127 (clone R34.34, Beckman Coulter), CRTH2 (clone BM16, BD Biosciences), CD19 (SJ25C1, BD Bioscience), CD3 (OKT3, Biolegend) or CD69 (clone FNSO, BioLegend), CD4 (clone RPA-T4, BD Bioscience), CXCR3 (clone 1C6, BD Bioscience) or CD3 (clone UCHT1, BD Biosciences), CXCR5 (clone RF8B2, BD Bioscience) and CD103 (clone Ber-ACT8, Biolegend). Intracellular stains were done after using a Fix/Perm kit (BD Biosciences) and included caspase-3 (clone C92-605, BD Bioscience) and BCL2 (clone 100, BD Bioscience).

Cells were surface-stained with 25 μl of the appropriate antibody panel at room temperature in the dark, for 20 min. Following the BD Bioscience Fix/Perm step, cells were stained with the corresponding intracellular panel for a minimum of 20 min in the dark before being fixed with 2% paraformaldehyde. Fixed cells were acquired on a four-laser BD Fortessa flow cytometer (CUBS and fresh blood samples) or a five-laser FACSAria Fusion (lung, chemokine and apoptosis experiment samples) within 24 h of processing.

Mouse lung cell isolation and preparation were performed as described previously[11]. In brief, mice were asphyxiated with CO_2 and lungs were perfused with heparin in saline. Lungs were minced and incubated in collagenase/DNase (Sigma-Aldrich) for 30 min at 37 °C. Lungs were pushed through a 70-μm nylon screen to release cells. Following red-blood-cell lysis, cells were used for flow cytometry analysis. The following antibodies were from TonBo Biosciences: CD127 (clone A7R34), CD3 (clone 145-2C11) and CD19 (clone 1D3). Antibodies purchased from eBioscience were: RORc(γt) (clone AFKJS-9) and Sca-I (clone D7). CD45 (clone 30-F11), CCR6 (clone 140706), IL-17 (TC11-18H10), streptavidin and CXCR5 (clone 2G8) were purchased from Becton Dickinson. The following antibodies were from Invitrogen: biotinylated NKp46, TER-119 (clone TER-119), CD11c (clone N418), IL-22 (clone 1H8PWSR) and CD5 (clone 53-7.3) and CD11b (clone M1/70) from BioLegend. Live/dead AQUA was purchased from ThermoFisher Scientific. For intracellular staining, fixation/permeabilization concentrate and diluent (eBioscience) were used to fix and permeabilize lung cells for 20 min. The cells were incubated overnight with the intracellular staining. Samples were run on a four-laser BD Fortessa flow cytometer. All flow cytometry data were analysed using FlowJo version 9.7.6 (TreeStar).

Adoptive transfer. Total ILCs (excluding ILC1, $CD45^{+}CD127^{+}Lin^{-}NK1.1^{-}$) were purified on a BD FACSJazz from the lungs of *Mtb*-infected C57BL/6 mice following enrichment for CD45 and staining with the above-mentioned antibodies. About 5,000 sorted and highly purified ILCs were intratracheally transferred into *Rag2*$^{-/-}$*Il2rg*$^{-/-}$ mice.

ELISA. The Quantikine ELISA assay for human CXCL13/BLC/BCA-1 was used to measure the amount of CXCL13 in the plasma of 19 participants before and after 6 months of successful anti-tuberculosis treatment. Standards, controls and samples were run in triplicate. Results were measured at 450 nm using the GlowMax-Multi detection system (Promega). Concentrations were determined based on the standard curve generated on GraphPad Prism version 6.0 (GraphPad Software). Protein levels of mouse cytokines (IL-17, IL-22 and IL-23) in culture supernatants were measured using mouse ELISA kits or multiplex according to the manufacturer's instructions (R&D Systems, MBL International Corporation).

In vitro chemotaxis assays. We sorted 10,000 human ILCs in duplicate (1 control and 1 experiment per individual) from PBMCs using the FACS panel described above, on a five-laser FACSAria Fusion. Cells were directly sorted into 100 μl of freshly prepared medium (HBSS containing 10% FBS) at 4 °C and transferred into the top well of a Corning HTS 24-well transwell plate. Bottom chambers of transwell plates were loaded with 600 μl of either medium alone, for controls, or medium containing 500 ng ml^{-1} recombinant human CXCL13 (R&D Systems), for experimental wells. Transwell plates were incubated for 2 h and then the aspirate from the bottom chamber was mixed with 50 μl of precision count beads (BioLegend) and acquired on a FACSAria Fusion. As antibody stains from the initial sort remained visible, ILC3s were identified and then counted using counting beads as per the manufacturers' instructions.

For the mouse chemotaxis assay, mouse ILCs (excluding ILC1, $CD45^{+}CD127^{+}Lin^{-}NK1.1^{-}$) were sorted from *Mtb*-infected C57BL/6 mice after CD45 enrichment within the total lung cells using the staining panel described

above, on a FACSJazz. Cells were directly sorted into 100 μl of freshly prepared medium (HBSS containing 10% FBS) at 4 °C and transferred into the top well of a Corning HTS 24-well transwell plate. Bottom chambers of transwell plates were loaded with 600 μl of either medium alone, for controls, or medium and 500 ng ml^{-1} of recombinant mouse CXCL13 (R&D Systems) for experimental wells. Transwell plates were incubated for 2 h and then the aspirate from the bottom chamber was stained using the ILC3 marker panel on a four-laser BD Fortessa flow cytometer to determine the exact number of ILC3s that migrated in response to the CXCL13 gradient.

Multiplex fluorescent immunohistology. Fluorescent immunohistology was performed on histological sections of tuberculosis-infected lung tissues that were either supplied by P. Ramdial or prepared in-house from formalin-fixed lung tissue following resections. Sections were dried overnight at 60 °C and then processed using an Opal four-colour Manual IHC kit (Perkin Elmer) as per the manufacturer's instructions with antibodies against CD20 (1:400), CD3 (1:400) and CD127 (1:100), VIP (1:100) and OSM (1:100) as primary antibodies. Slides were scanned on a Zeiss Axio Observer microscope using TissueFAXS imaging software (Tissuegnostics) and analysed using TissueQuest analysis software (Tissuegnostics).

Whole transcriptome amplification and RNA sequencing. ILC2 and ILC3 populations were sorted from lung tissue from five participants with tuberculosis and two participants with cancer (who acted as a control) using a five-laser FACSAria Fusion. A validated 17-colour FACS panel (Extended Data Fig. 1) and stringent gating was used to identify ILC2 and ILC3 populations in these samples. Cells were directly sorted into RLT buffer (Qiagen) containing 1% β-mercaptoethanol. Lysates were snap-frozen on dry ice and stored at −80 °C. As input numbers were low (50–1,385 cells), thawed lysate was split into three technical replicates for each sample to increase the probability of successful amplification. RNA extraction, cDNA conversion and whole-transcriptome amplification was carried out as previously described using Smart-seq2[9]. The quality of the amplified product was confirmed using a high-sensitivity DNA analysis kit and a 2100 BioAnalyzer (Aligent Technologies), and concentrations were measured using a Qubit assay kit (ThermoFisher Scientific). Diluted samples were tagmented, amplified and individually barcoded using a Nextera XT DNA Library prep kit (Illumina), cleaned using AMPure XP SPRI beads (Beckman Coulter) and sequenced on a NextSeq 500 (Illumina) using 30 × 30 PE reads with 8 × 8 index reads to an average depth of 14.9×10^6 reads.

mRNA expression. RNA was extracted from the sorted mouse ILCs ($CD45^+CD127^+Lin^-NK1.1^-$) using the Qiagen RNeasy Mini kit (Qiagen). cDNA was generated using ABI reverse transcription reagents (ABI, ThermoFisher Scientific) and RT–PCR was run on a ViiA7 Real-Time PCR system (Life Technologies, ThermoFisher Scientific). The relative expression of *Ccr6*, *Rorγt* and *Ahr* in sorted ILCs was calculated over expression of *Gapdh* in each sample. The primer and probe sequences for mouse *Gapdh* were previously published[11]. The primer and probes for mouse *Ccr6*, *Rorγt* and *Ahr* were purchased from Applied Biosystems.

RNA-sequencing data analysis. Sequencing data from the NextSeq 500 were demultiplexed and aligned against hg38 using TopHat[27], and expression values, in counts, were generated in RSEM[28] for every sample. Samples with fewer than 10^6 aligned transcriptionally reads, or fewer than 10,000 measured genes, and genes expressed with fewer than five counts in fewer than four samples were discarded from subsequent analysis.

Differential expression analysis was performed in R (build 3.3.2) using the DESeq2 package[29] (version 1.14.1) on ILC2s and ILC3s between samples (and replicates) from five individuals with tuberculosis and two individuals without tuberculosis. The DESeq2 results can be found in Supplementary Tables 1, 2; hits with FDR $q < 0.01$ were considered differentially expressed for downstream analyses. Differentially expressed genes and their significances and log-transformed fold changes for each comparison were then processed using Ingenuity Pathway Analysis (IPA) (Qiagen, https://www.qiagenbioinformatics.com/products/ingenuity-pathway-analysis) to populate lists of predicted upstream drivers (Supplementary Tables 3, 4). Upstream driver plots were generated from the 'upstream analysis' in IPA; hits with 'molecule type' including the word 'chemical', '*P*-value of overlap' > 0.01, and number of 'target molecules in data set' < 3 were excluded from plotting. The OSM upstream driver network was created using the mechanistic networks generated by IPA, using $P < 0.01$ for overlap significance. The downstream driver network for genes known to interact with OSM was generated using the ClueGO plugin[30] (version 2.3.3) in Cytoscape (version 3.3.0) with the following ontologies: Gene Ontology (GO) biological process, GO immune system process, KEGG (Kyoto Encyclopedia of Genes and Genomes) and Reactome pathways. Only pathways with significance of $P < 0.01$ after Benjamaini–Hochberg correction are shown, and a kappa score threshold of 0.45 was used to merge terms. The downstream pathway bar chart was generated using the 'downstream pathways' in IPA, for which large categories were manually annotated. All sequencing data have been deposited and are available from the Gene Epression Omnibus (GEO) repository, accession number GSE131031.

ILC3 staining and quantification. Immunohistochemical staining of human, non-human primate and mouse formalin-fixed paraffin-embedded (FFPE) lung sections were initially dewaxed in xylene before hydrating with decreasing graded alcohol and methanol passages. Antigens were retrieved by heat treatment in 92 °C and EDTA buffer pH 8. Tissue staining with antibodies against RORγt (clone 6F3.1, Millipore for mouse; clone Q31-378, BD Bioscience for non-human primate and human), CD3 (clone SP7, ThermoFisher Scientific for human, non-human primate and mouse), PAX5 (clone 24/Pax-5, BD Pharmingen, for human and non-human primate) or B220 (clone RA3-6B2, BD Pharmingen) was performed for 1 h in a humid chamber. Tissues were washed in Tris-buffered saline pH 7.4–7.6 before incubation with secondary antibody (Novocastra Post Primary, Leica) and polymer (Novolink Polymer, Leica). To develop the reaction, tissues were incubated with 3,3′-diaminobenzidine chromogen (DAB, Leica). Single-stained sections (PAX5, B220) were incubated with DAB for 5 min and double-stained sections (RORγt and CD3) were incubated overnight. Tissues were counterstained with haematoxylin and rinsed in water. All tissues were mounted with coverslips using glycerol mounting medium. $CD3^-ROR\gamma t^+$ ILC3s were quantified in the slides. Images were analysed manually by counting the number of ILC3s per field. The analysis was done in a blinded manner.

Immunofluorescence staining and in situ hybridization. Mouse lung lobes were perfused with 10% formalin, fixed and paraffin embedded. In brief, the FFPE sections were processed to remove paraffin and then hydrated in 96% alcohol and phosphate-buffered saline. Antigens were retrieved with a DakoCytomation Target Retrieval Solution (Dako) and non-specific binding was blocked using 5% (v/v) normal donkey serum and Fc block (BD Pharmingen). Sections were then probed with anti-B220 (clone RA3-6B2, BD Pharmingen; dilution, 1:100) and anti-CD3 (clone M-20, Santa Cruz Biotechnology, Santa Cruz, CA; dilution, 1:100) antibodies to detect B cell follicle formation. For B cell follicles analyses, follicles were outlined with the automated tool of the Zeiss Axioplan 2 microscope (Zeiss), and total area and average size were calculated in μm^2.

To detect $CD3^-ROR\gamma t^+$ ILC3s and $CD20^+$ B cells in lungs of non-human primates[11] and humans infected with tuberculosis, slides were incubated with primary goat anti-CD3ε (clone M-20, Santa Cruz Biotechnology), mouse anti-human RORγt (clone 6F3.1, Milipore Sigma-Aldrich) and rabbit anti-human CD20 (LS-B2605-125, Lifespan Biosciences) antibodies. To detect $CD3^-ROR\gamma t^+$ ILC3s and $CD20^+$ B cells in mouse lungs infected with *Mtb*, slides were incubated with primary goat anti-CD3ε (clone M-20, Santa Cruz Biotechnology), monoclonal rabbit anti-mouse RORγt (clone EPR20006, Abcam) and APC-rat anti-mouse CD45R (B220, clone RA3-6B2, BD Biosciences). Slides were incubated with primary antibodies overnight at room temperature in a humid chamber. The next day, slides were briefly washed in PBS, and primary antibodies were revealed with Alexa Fluor 568-conjugated donkey anti-goat IgG (A11057, ThermoFisher Scientific), FITC-conjugated donkey anti-mouse IgG (715-095-150, Jackson ImmunoResearch Laboratories), biotin-conjugated donkey anti-rabbit (711-065-162, Jackson ImmunoResearch Laboratories) or Alexa Fluor 568-conjugated donkey anti-goat IgG (A11057, ThermoFisher Scientific) and Alexa Fluor 488-conjugated donkey anti-rabbit IgG (711-546-152, Jackson ImmunoResearch Laboratories) for human or non-human primate slides or mouse slides, respectively. Finally, streptavidin Alexa Fluor 680 (S32358, ThermoFisher Scientific) was added to the slides to visualize CD20 for human or non-human primate sections. Slides were washed in PBS and mounted with Vectashield antifade mounting medium with DAPI (Vector Laboratories, H-1200). ILC3s were counted in 3−5 random 200× fields in each individual slide. Representative 200× images were taken with Axioplan Zeiss Microscope and recorded with a Hamamatsu camera.

FFPE lung sections were subjected to in situ hybridization with the mouse *Cxcl13* probe using the RNAscope 2.5HD Detection Kit (Brown staining) as per the manufacturer's instructions (Advanced Cell Diagnostics). The representative images were captured with the Hamamatsu Nanozoomer 2.0 HT system with NDP scan image acquisition software. The $Cxcl13^+$ area and total area per lobe was quantified in a 40× magnification. The ratio was calculated by dividing the $Cxcl13^+$ area by total area on each lobe.

Statistical analyses. Where MFI data were measured at different time points, MFI was converted to final relative MFI by normalizing each measurement to an internal control to standardize these measurements over time[31]. The Mann–Whitney *U*-test was used to determine statistical significance between two groups, with the exception of the human transwell data, which were analysed by one-tailed Wilcoxon signed-rank test; whereas significance between more than two groups was calculated using the Dunn's multiple comparisons test or a Mann–Whitney *U*-test with Bonferroni corrections. Comparisons between matched samples for which data were paired were analysed with the Wilcoxon matched-pairs signed-rank test. All statistical analyses were performed using GraphPad Prism version 6.0d (GraphPad Software).

For mouse studies, differences between the means of two groups were analysed using two-tailed Student's *t*-test in Prism 5 (GraphPad). Differences between the means of three or more groups were analysed using one-way ANOVA with Tukey's post test. $P < 0.05$ was considered significant.

Reporting summary. Further information on research design is available in the Nature Research Reporting Summary linked to this paper.

Data availability

All relevant data are available from the corresponding authors upon reasonable request. RNA-sequencing data that support the findings of this study have been deposited in the Gene Expression Omnibus (GEO) repository, accession number GSE131031.

27. Trapnell, C. et al. Differential gene and transcript expression analysis of RNA-seq experiments with TopHat and Cufflinks. *Nat. Protoc.* **7**, 562–578 (2012).
28. Li, B. D. & Dewey, C. N. RSEM: accurate transcript quantification from RNA-seq data with or without a reference genome. *BMC Bioinformatics* **12**, 323 (2011).
29. Love, M. I., Huber, W. & Anders, S. Moderated estimation of fold change and dispersion for RNA-seq data with DESeq2. *Genome Biol.* **15**, 550 (2014).
30. Bindea, G. et al. ClueGO: a Cytoscape plug-in to decipher functionally grouped gene ontology and pathway annotation networks. *Bioinformatics* **25**, 1091–1093 (2009).
31. Upreti, D., Pathak, A. & Kung, S. K. Development of a standardized flow cytometric method to conduct longitudinal analyses of intracellular CD3ζ expression in patients with head and neck cancer. *Oncol. Lett.* **11**, 2199–2206 (2016).

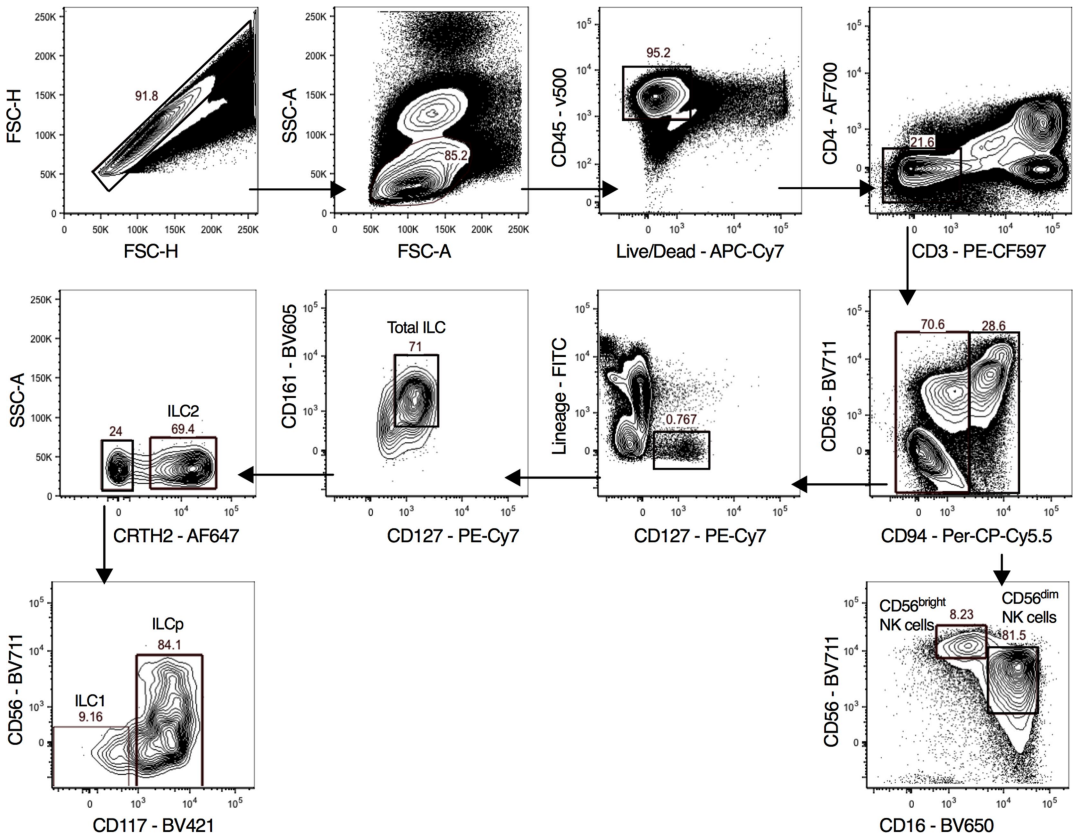

Extended Data Fig. 1 | Hierarchical gating strategy used to identify lymphocyte populations in human blood and lung samples. Single cells from blood ($n = 68$) or lung samples ($n = 42$) from human participants were processed for flow cytometry, and all doublets were excluded. Cells were gated as lymphocytes, live, $CD45^+$ and $CD3^+$ T cells or $CD3^-$ cells. $CD3^-$ cells were gated on CD56 and CD94. $CD94^+$ cells are NK cells and were further subgated as $CD16^-CD56^{high}$ NK cells or $CD16^+CD56^{low}$ NK cells. ILCs in the $CD94^-$ fraction were $CD127^+$ and negative for all lineage markers: CD4, CD11c, CD14, CD19, CD34, FcER1, BDCA2, TCRαβ and TCRγδ. Total ILCs were $CD127^+CD161^+$, ILC2s were $Lin^-CD127^+CRTH2^+$ cells. ILC1s were $Lin^-CD127^+CRTH2^-CD56^-CD117^-$ cells. ILC3 were $Lin^-CD127^+CRTH2^-CD117^+$ cells with variable CD56 expression.

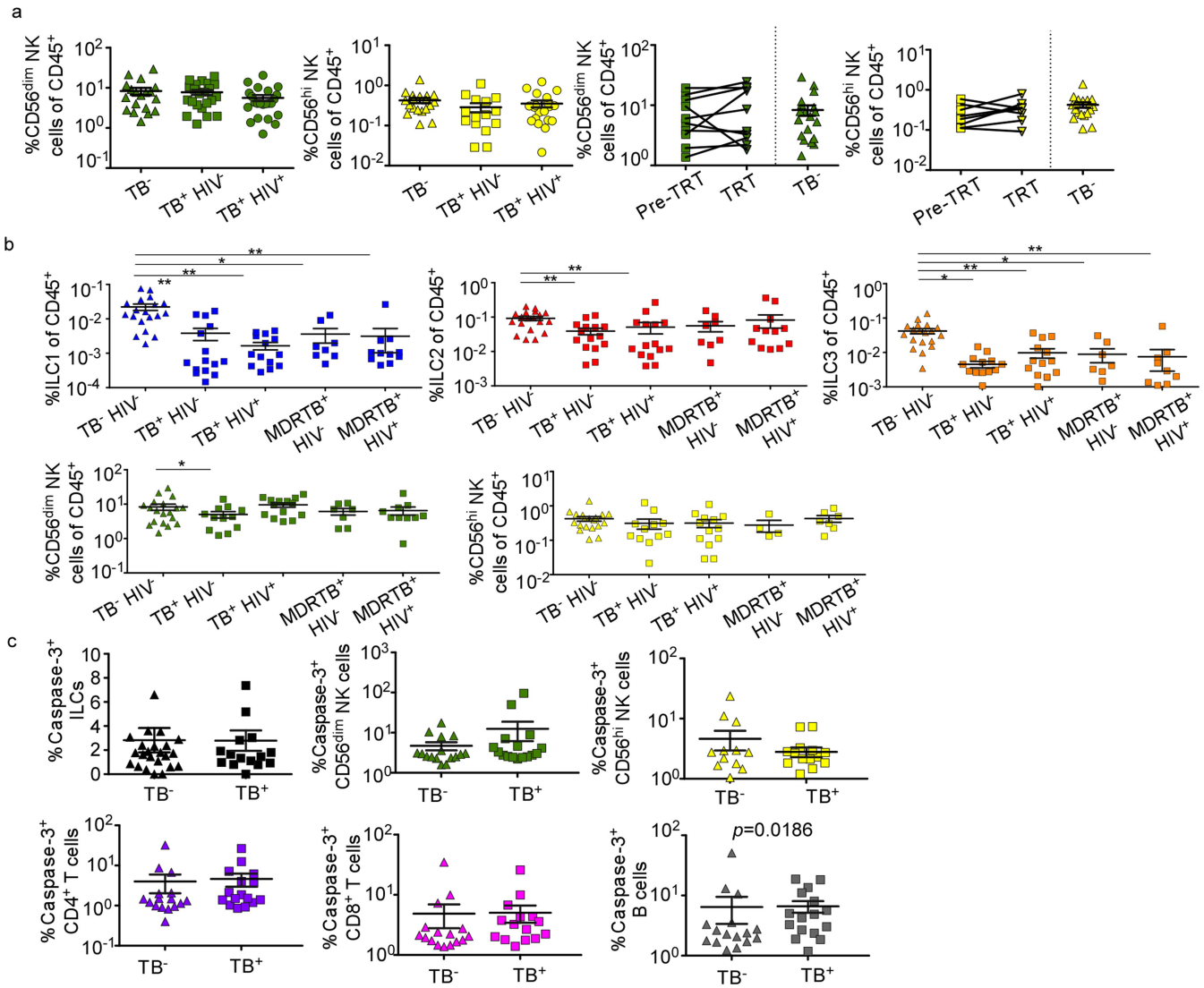

Extended Data Fig. 2 | ILC depletion seen in participants with tuberculosis is not affected by tuberculosis drug resistance or concurrent infection with HIV. a, The frequencies of the two main circulating NK populations, $CD16^{+}CD56^{low}$ and $CD16^{-}CD56^{high}$ were measured in human participants with tuberculosis ($n = 35–45$) and healthy controls ($n = 19$) by flow cytometry. NK cell frequencies in paired samples taken from the same participant with tuberculosis before and after 6 months of standard and successful tuberculosis therapy were also determined by flow cytometry ($n = 8–11$). **b**, Percentages of blood ILC1s, ILC2s, ILC3s, $CD56^{low}$ NK cells and $CD56^{high}$ NK cells were measured in control subjects who did not have tuberculosis (TB) or HIV ($TB^{-}HIV^{-}$, $n = 19$), participants with tuberculosis and without HIV ($TB^{+}HIV^{-}$, $n = 13–15$) and with tuberculosis and HIV coinfection ($TB^{+}HIV^{+}$, $n = 12–15$), and participants with multi-drug-resistant tuberculosis without HIV ($MDRTB^{+}HIV^{-}$, $n = 4–8$) and with multi-drug-resistant tuberculosis with HIV coinfection ($MDRTB^{+}HIV^{+}$, $n = 7–12$). Significance is calculated by a Dunn's multiple comparison test. $^{*}P < 0.05$, $^{**}P < 0.01$. c, Capase-3 expression in circulating lymphocytes from peripheral blood of participants with tuberculosis ($n = 14–16$) and controls ($n = 15–24$) was done by flow cytometry. Significance calculated using a Mann–Whitney *U*-test. Data are mean ± s.d and individual values.

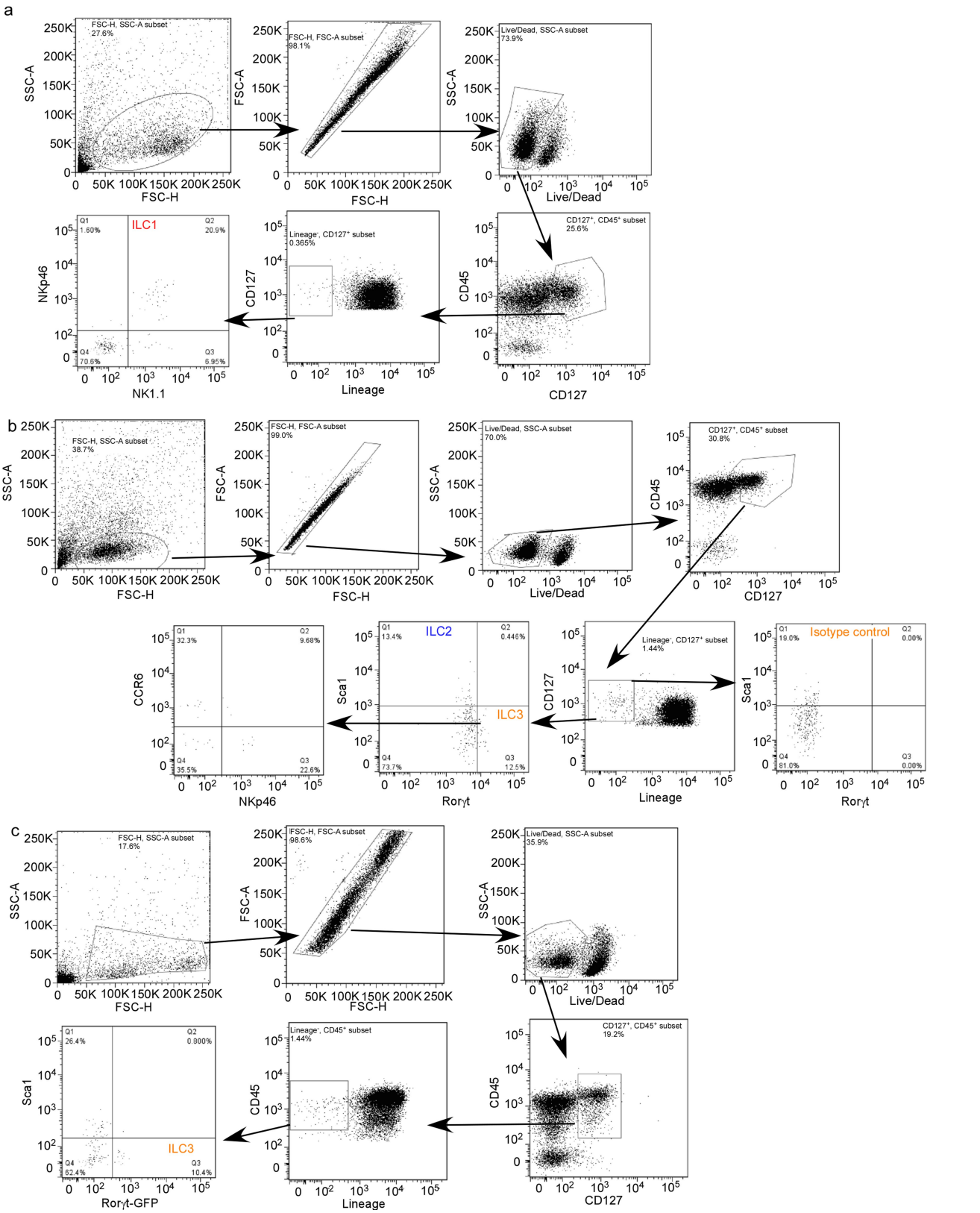

Extended Data Fig. 3 | Hierarchical gating strategy used to identify ILC populations in mouse lungs. a–c, C57BL/6 mice were aerosol infected with approximately 100 CFU *Mtb* and lungs were collected at different d.p.i. and flow cytometry analysis was carried out on single-cell suspensions. **a**, **b**, Flow gating strategies for ILC1s ($CD45^+CD127^+Lin^-NKp46^+NK1.1^+$), ILC2s ($CD45^+CD127^+Lin^-NK1.1^-Sca1^+$) and ILC3 ($CD45^+CD127^+Lin^-NK1.1^-Ror\gamma t^+$) and NKp46-expressing ($CD45^+CD127^+Lin^-NK1.1^-Ror\gamma t^+NKp46^+$) ILC3s are shown. **c**, Rorγt–GFP mice were aerosol-infected with approximately 100 CFU *Mtb* and lungs were collected at 14 d.p.i. ILC3 ($CD45^+CD127^+Lin^-NK1.1^-GFP^+$) populations were quantified using flow cytometry.

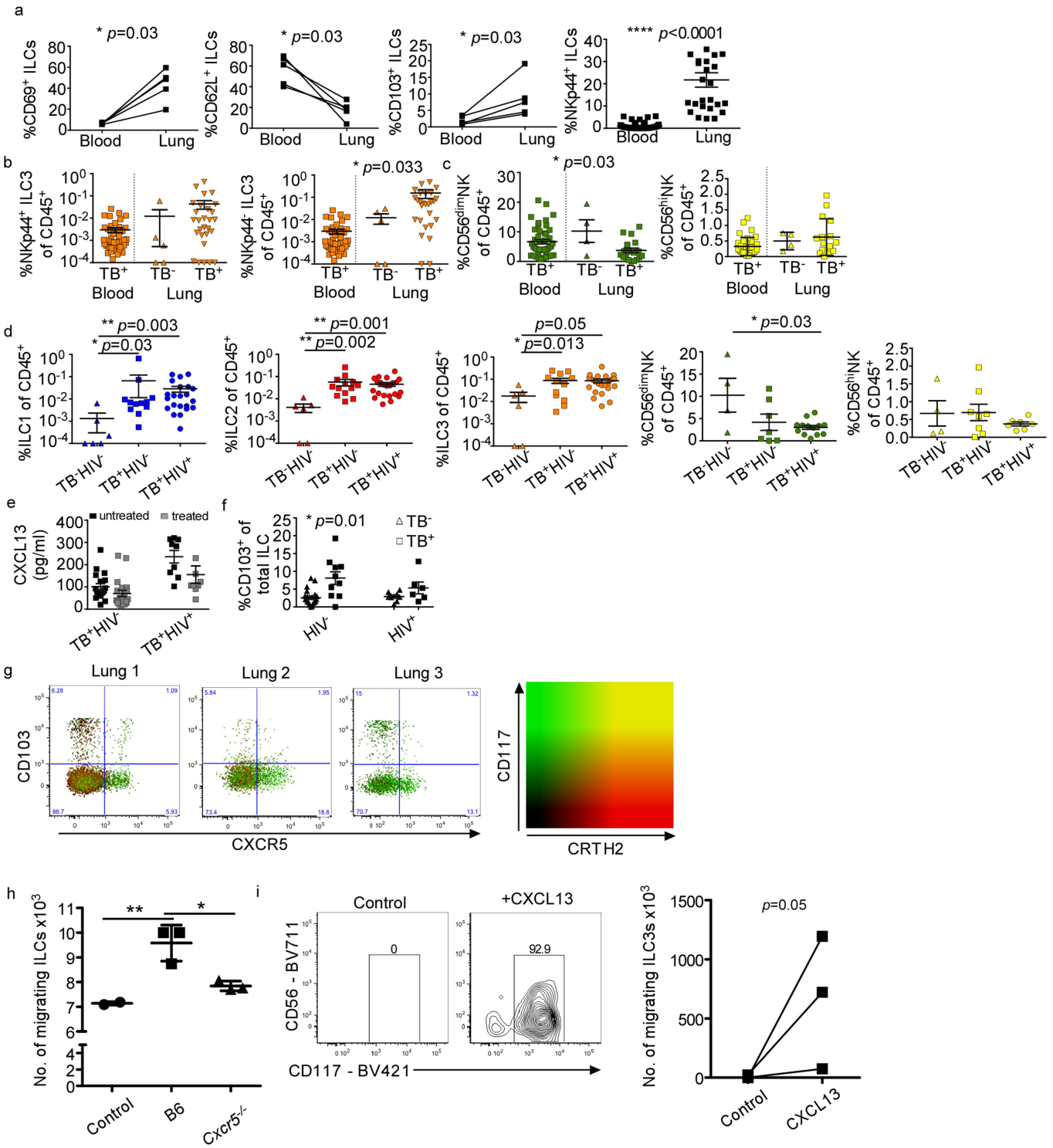

Extended Data Fig. 4 | See next page for caption.

Extended Data Fig. 4 | Pulmonary ILCs are tissue-resident cells and express markers of migration. a, CD69, CD103, CD62L and NK-p44 expression on the circulating ILCs in human peripheral blood and lung tissue were measured by flow cytometry. Percentage of total human ILCs expressing these markers in paired samples of participants with tuberculosis shown (paired samples $n = 5$; NK-p44 expression unpaired samples, lung $n = 26$; blood $n = 34$). Significance of CD69, CD103 and CD62L expression was calculated using a one-way Wilcoxon matched-pairs test. Significance of NK-p44 expression was analysed using an unpaired Mann–Whitney *U*-test. **b**, **c**, NK-p44 and CD56 expression were measured in tuberculosis-infected lung tissues in comparison to control samples. Significance is analysed using a unpaired Mann–Whitney *U*-test (**b**) and a Kruskal–Wallis test with adjustments for multiple comparisons (**c**). **d**, Percentages of ILC1, ILC2, ILC3, $CD56^{low}$ NK cells, and $CD56^{high}$ NK cells in human lung tissue were measured by flow cytometry $TB^{-}HIV^{-}$ control subjects ($n = 4$–6), participants with tuberculosis without HIV ($TB^{+}HIV^{-}$, $n = 7$–13) and with tuberculosis with HIV coinfection ($TB^{+}HIV^{+}$, $n = 7$–22). **e**, CXCL13 protein levels were measured in the plasma of participants with tuberculosis without ($n = 18$–20) and with HIV coinfection($n = 9$). Significance is calculated by Mann–Whitney *U*-test (no significance after Bonferonni correction). **f**, Frequencies of $CD103^{+}$ ILCs were measured by flow cytometry in the blood of $TB^{-}HIV^{-}$ control subjects ($n = 24$), participants with tuberculosis without ($n = 10$) and with HIV coinfection ($n = 5$). Significance is analysed using a Mann–Whitney *U*-test with Bonferroni corrections (only values that were significant after correction are shown). **g**, Representative FACS plots showing two distinct subpopulations of CD103- and CXCR5-expressing ILCs measured in lung tissues from three subjects with tuberculosis; in these populations most CXCR5-expressing cells are $CD117^{+}$ ILC3s and $CD103^{+}$ lung ILCs are a combination of $CD117^{+}$ ILC3s, $CRTH2^{+}$ ILCs and $CD117^{-}CRTH2^{-}$ cells. Green, $CD117^{+}$; red, $CRTH2^{+}$. **h**, C57BL/6 mice were aerosol-infected with approximately 100 CFU *Mtb* and lungs were collected at 14 d.p.i. Lung ILCs were sorted from single-cell suspensions (ILCs: $CD45^{+}CD127^{+}Lin^{-}NK1.1^{-}$).The ability of sorted ILCs to migrate towards medium alone or a gradient of mouse CXCL13 was quantified in a transwell migration assay. $n = 3$–5 biological replicates. Significance is calculated by one-way ANOVA, $^{*}P < 0.05$, $^{**}P < 0.01$. **i**, Human ILC3s sorted from lungs migrated in response to recombinant human CXCL13 in transwell migration assays. Significance is calculated by one-tailed Wilcoxon signed-rank test. Data are paired values (**a**, left three graphs and **i**, right) or mean ± s.d. and individual values (**b**–**f**, **h**).

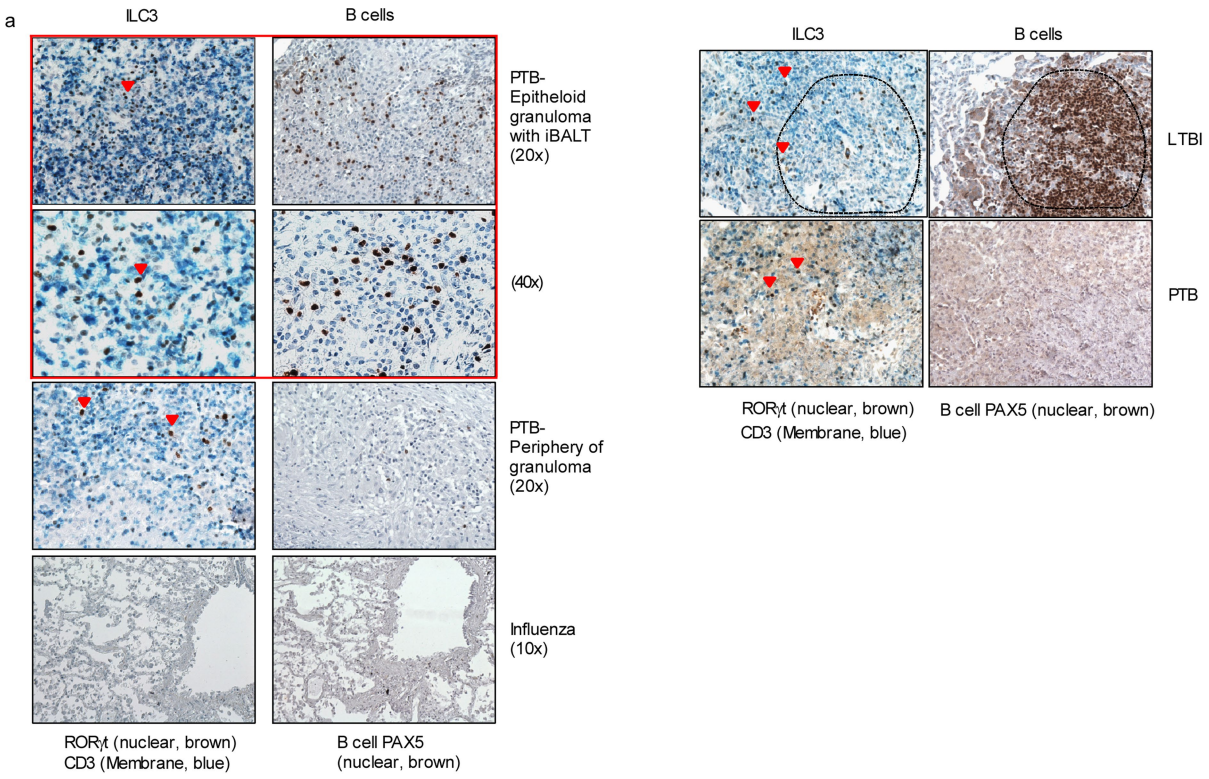

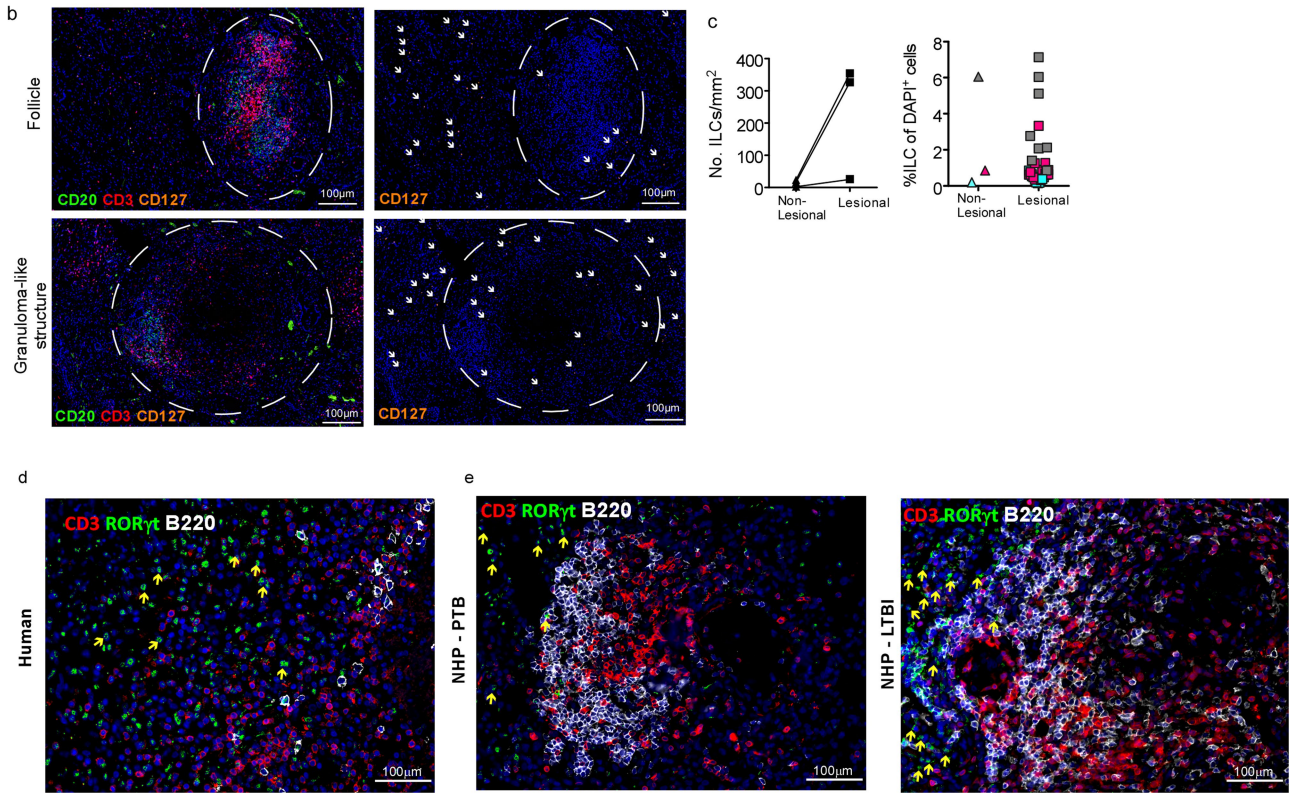

Extended Data Fig. 5 | See next page for caption.

Extended Data Fig. 5 | ILC3s localize within lymphoid follicles during tuberculosis. a, IHC staining of nuclear RORγt, CD3 and PAX5 on FFPE lung tissues from human participants with pulmonary tuberculosis or influenza (left) or macaques with latent tuberculosis infections and pulmonary tuberculosis (right). **b**, Representative fluorescent immunohistology scans of tuberculosis-infected human lung tissues, with CD20 (FITC), CD3 (PE–Texas Red) and CD127 (PE–Cy5). $CD3^{-}CD127^{+}$ ILCs are present adjacent to follicles (top) and granuloma-like structures (bottom). **c**, Cumulative total ILCs per mm^2 of lung tissue (left), in histological sections from 3 different patients with tuberculosis, are increased in structures of tuberculosis histopathlogy (combined lesional tissue) in comparison to the remainder of unaffected tissue (non-lesional). However, percentages of ILCs per total cell number ($DAPI^{+}$ cells) (right) are not different between regions of interest (lesional tissue, $n = 31$ lesions) and unaffected tissue (non-lesional, $n = 3$ patients). **d**, **e**, ILC3 immunofluorescence analysis of nuclear RORγt, B220 and CD3 in FFPE lung tissues from human participants with pulmonary tuberculosis (**d**) and macaques (**e**) with pulmonary tuberculosis (PTB) and latent tuberculosis infections (LTBI).

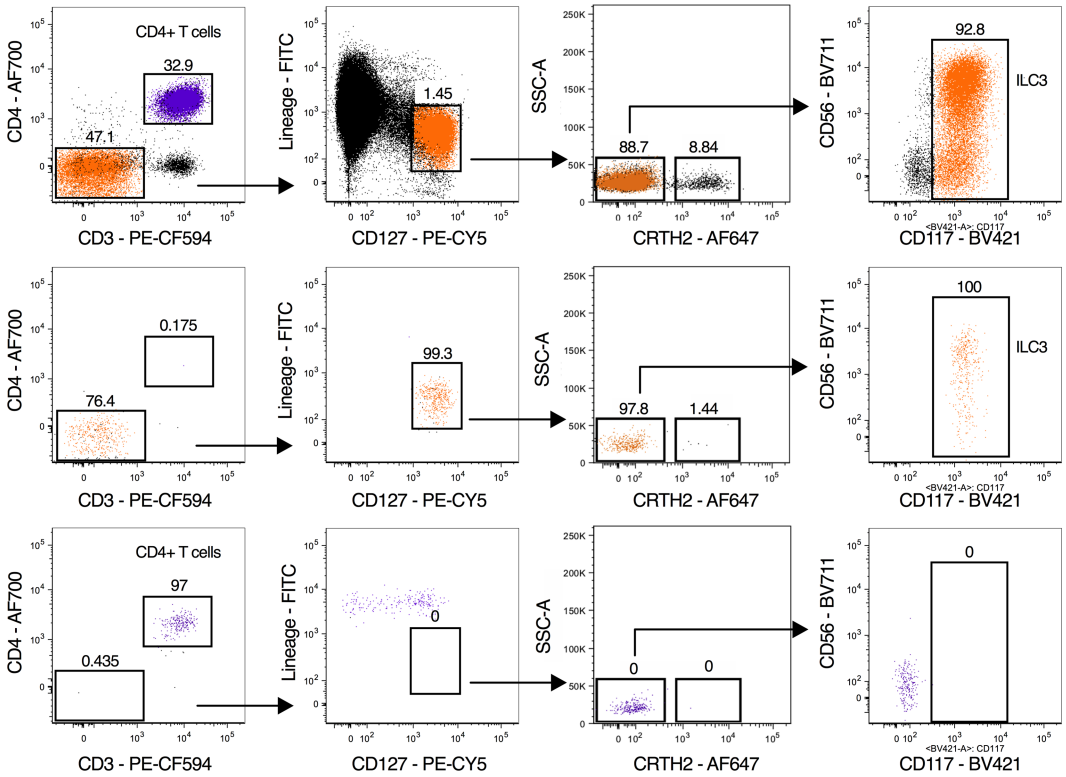

Extended Data Fig. 6 | Sort purity of human ILC3s and CD4$^+$ T cells. ILC3s and CD4$^+$ T cells were sorted from human PBMCs and reflowed back into FACSAria Fusion to confirm purity. Purity of ILC3s was confirmed to be 100% and the CD4$^+$ T cell sort was 97% pure.

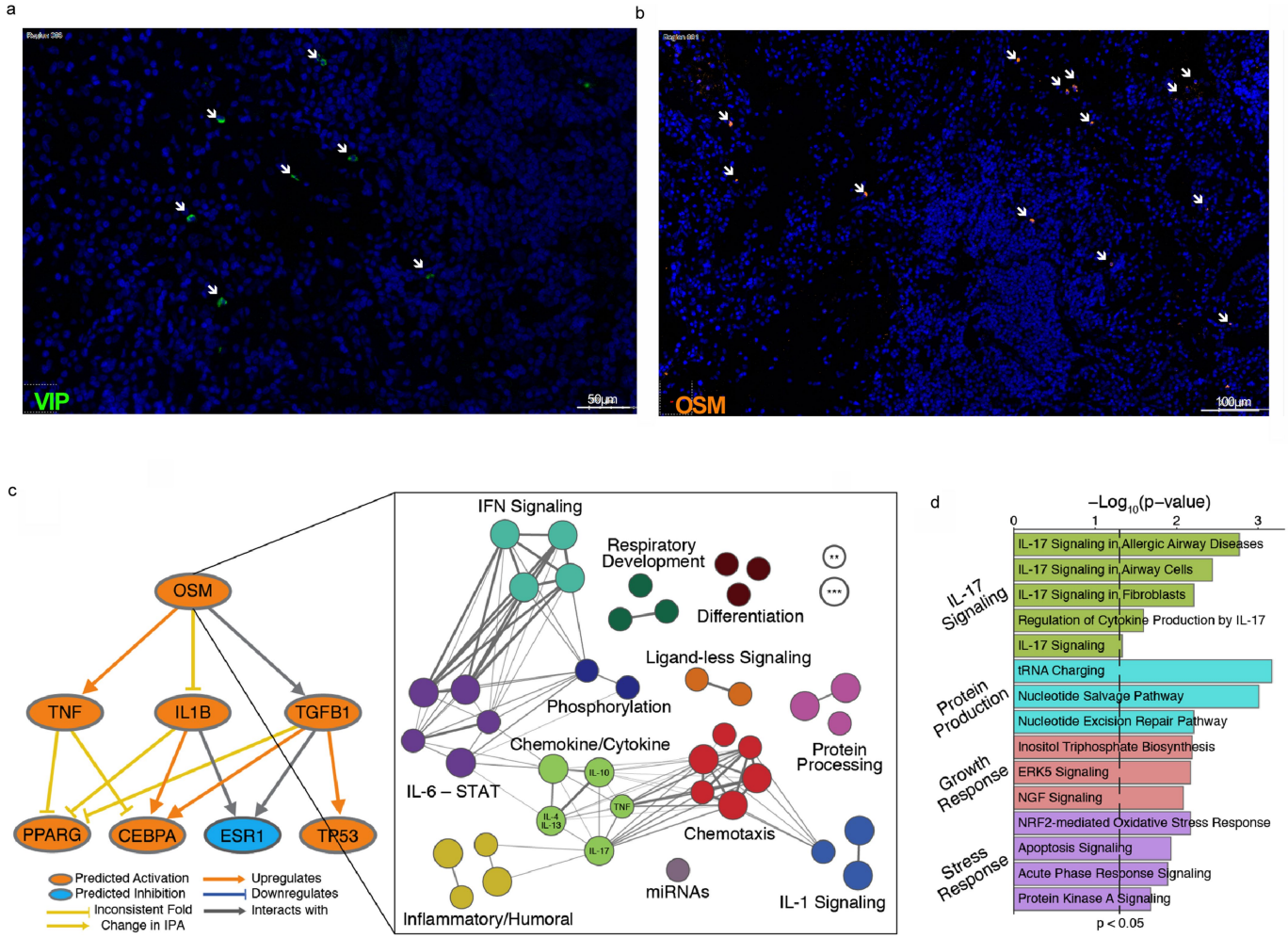

Extended Data Fig. 7 | VIP and OSM are expressed within human lung tissue infected with tuberculosis. a, **b**, VIP (**a**) and OSM (**b**) protein expression was confirmed in situ in human lung tissues infected with tuberculosis using multiplexed fluorescent immunohistology. **c**, The network of upstream drivers enriched in the differentially expressed genes in sorted ILC3s between tuberculosis-infected and uninfected samples are shown. Inset, GO network generated over the genes identified as downstream of OSM by IPA ($n = 64$, see Methods). Each node represents a specific GO, KEGG or Reactome term (Supplementary Table 4). Broad categories of pathways are annotated. Line width and darkness correspond to number of shared genes between nodes. Node size, $^{**}P < 0.01$; $^{***}P < 0.001$. **d**, Select predicted downstream pathways enriched in the differentially expressed genes in ILC3s between tuberculosis-infected and uninfected samples are shown.

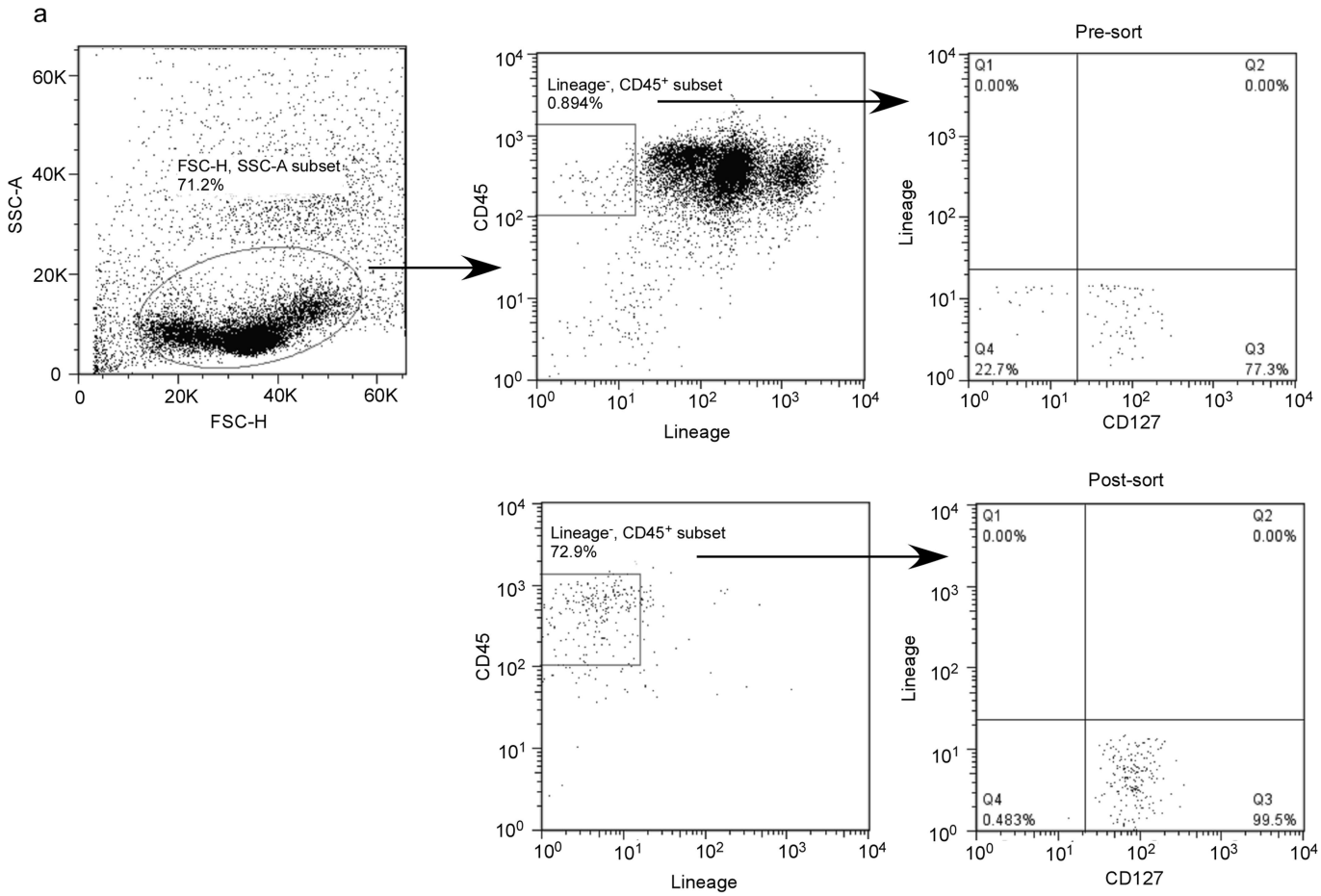

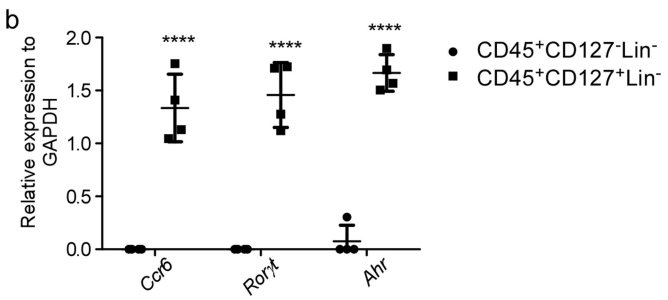

Extended Data Fig. 8 | Sorting purity of mouse ILCs. a, C57BL/6 mice were aerosol-infected with approximately 100 CFU *Mtb* and lungs were collected at 5 d.p.i. The lung CD45 population was enriched by using CD45 microbeads. CD45-enriched cells were stained and lung ILCs ($CD45^+CD127^+Lin^-NK1.1^-$) were purified by using FACSJazz. Sort purity is shown here. **b**, mRNA expression of *Ccr6*, *Rorγt* and *Ahr* relative to *Gapdh* in the purified ILCs ($CD45^+CD127^+Lin^-NK1.1^-$) and non-ILC population ($CD45^+CD127^-Lin^-NK1.1^-$) were quantified by RT–PCR. Significance is calculated by two-way ANOVA, $^{****}P < 0.0001$. Data are mean ± s.d. and individual values.

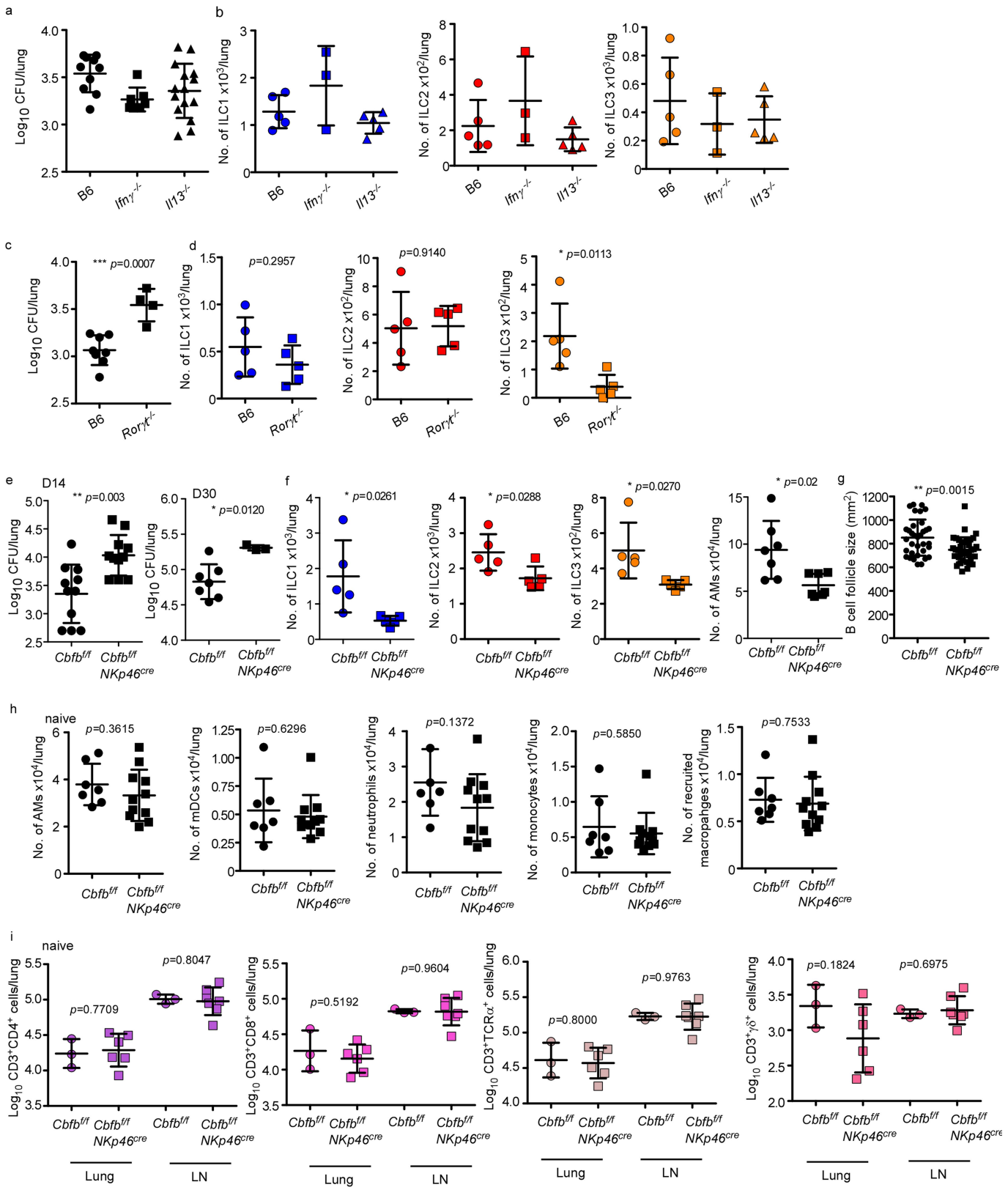

Extended Data Fig. 9 | See next page for caption.

Extended Data Fig. 9 | ILC1s and ILC2s are dispensable, while ILC3s are required for early protection against tuberculosis. a–**d**, C57BL/6 ($n = 5$–10), *Ifng*$^{-/-}$ ($n = 3$–7), *Il13*$^{-/-}$ ($n = 5$–15) and *Ror*$\gamma t^{-/-}$ ($n = 4$–5) mice were aerosol-infected with approximately 100 CFU *Mtb*. **a**, **c**, At 14 d.p.i., the bacterial burden was measured in the lungs by plating on 7H11 agar plates for 14 days. **b**, **d**, Numbers of lung ILC1s, ILC2s and ILC3s were quantified by flow cytometry. Significance is calculated by one-way ANOVA (**a**, **b**) or Student's *t*-test (**c**, **d**). **e**, *Cbfb*$^{f/f}$*Nkp46*^{cre} and *Cbfb*$^{f/f}$ mice were aerosol-infected with approximately 100 CFU *Mtb* and at 14 and 30 d.p.i. the bacterial burden was determined in the lungs by plating ($n = 5$–11 *Cbfb*$^{f/f}$ mouse; $n = 3$–11 *Cbfb*$^{f/f}$*Nkp46*^{cre} mouse). **f**, Numbers of lung ILC1s, ILC2s, ILC3s and alveolar macrophages were determined by flow cytometry. **g**, FFPE lung sections from 30 d.p.i. *Mtb*-infected mice were stained with antibodies against B220 and CD3, and the average size of B cell follicles was quantified. **h**, **i**, Tissues from uninfected *Cbfb*$^{f/f}$*Nkp46*^{cre} and *Cbfb*$^{f/f}$ mice were collected, and lung and lymph nodes were analysed for the different myeloid (**h**; alveolar macrophages, myeloid dendritic cells (mDCs), neutrophils, monocytes and recruited macrophages) and T cell (**i**; $CD3^+CD4^+$, $CD3^+CD8^+$, $CD3^+TCR\alpha^+$, $CD3^+\gamma\delta^+$) populations by flow cytometry. Significance is calculated by Student's *t*-test. Data are mean ± s.d. and individual values. All experiments were replicated at least twice.

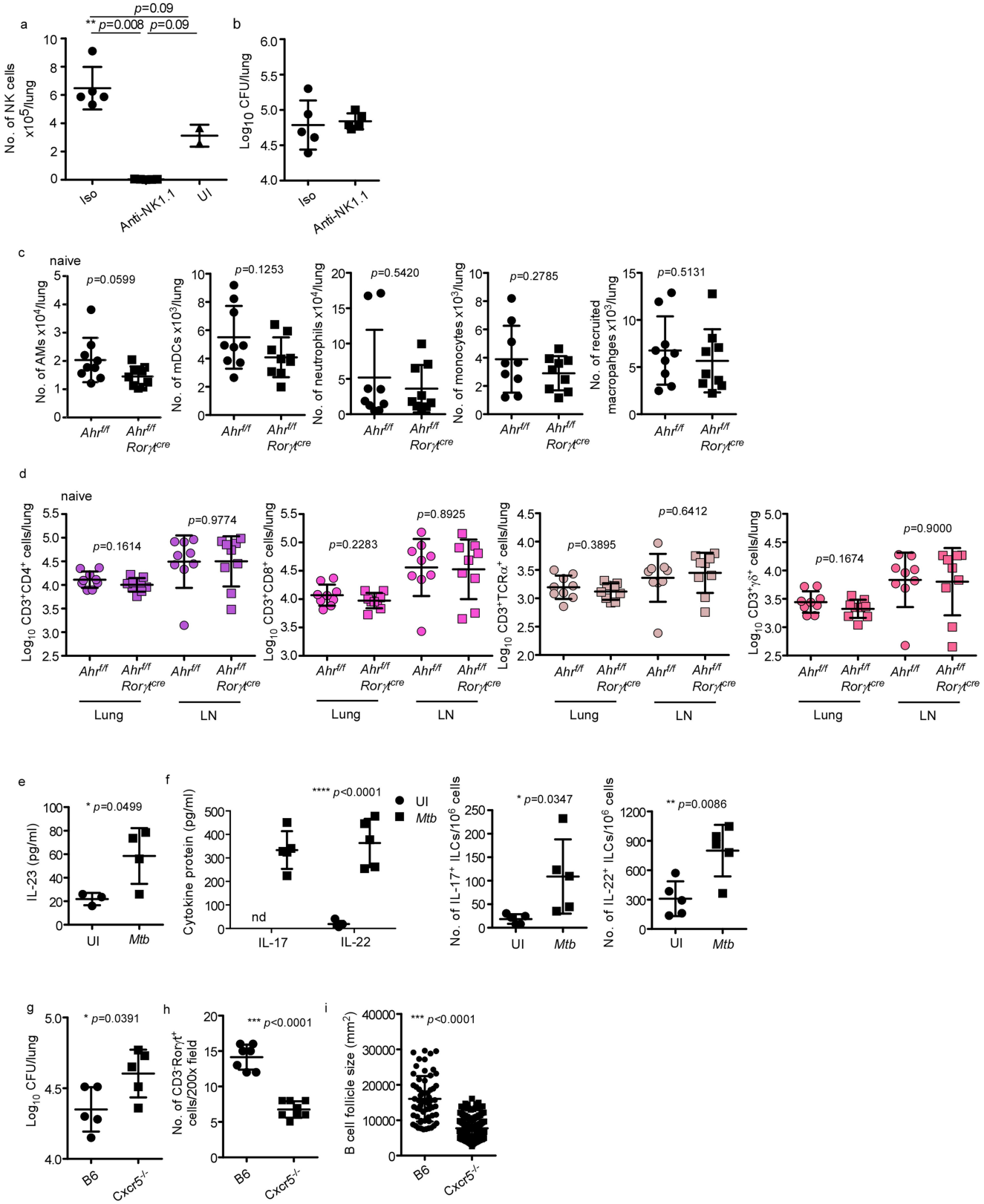

Extended Data Fig. 10 | See next page for caption.

Extended Data Fig. 10 | IL-17 and IL-22 are produced by lung ILCs following *Mtb* infection and mediate protection through the CXCR5 axis. C57BL/6 mice were aerosol-infected with approximately 100 CFU *Mtb* and treated with isotype ($n = 5$ mice) or anti-NK1.1 ($n = 5$ mice, PK126, 100 μg) antibodies every 3 days. **a**, Lung NK cells were determined following treatment with isotype or anti-NK1.1 antibodies at 30 d.p.i. by flow cytometry. **b**, Lung bacterial burden was assessed at 30 d.p.i. **a**, **b**, Significance calculated by Student's *t*-test. **c**, **d**, Tissues from uninfected $Ahr^{f/f}$ and $Ahr^{f/f}Ror\gamma t^{cre}$ mice were collected, and lung and lymph nodes were analysed for the different myeloid (**c**; alveolar macrophages, myeloid dendritic cells, neutrophils, monocytes and recruited macrophages) and T cell (**d**; $CD3^+CD4^+$, $CD3^+CD8^+$, $CD3^+TCR\alpha^+$, $CD3^+\gamma\delta^+$) populations by flow cytometry ($n = 9$ mice per group). **e**, Lung cells from C57BL/6 mice were infected in vitro with *Mtb* (MOI of 0.1) and IL-23 protein levels were measured in supernatants on 5 d.p.i. and compared to uninfected (UI) cells. $n = 3$ uninfected dishes, $n = 4$ *Mtb*-infected dishes. **f**, Left, lung cells from C57BL/6 mice were infected in vitro with *Mtb* (MOI of 0.1) as in **e** and stimulated with recombinant (r)IL-23, rIL-1β, and the protein levels of IL-22 and IL-17 were measured in supernatants and compared with levels in uninfected cells. Right, numbers of IL-17- and IL-22-producing ILCs were measured by flow cytometry. **g**, C57BL/6 and $Cxcr5^{-/-}$ mice were aerosol-infected with around 100 CFU *Mtb* and at 30 d.p.i. the bacterial burden was determined in the lungs by plating ($n = 5$ mice per group). **h**, ILC3 quantification in FFPE lung sections was carried out by staining with antibodies against CD3, B220 and Rorγt, and the number of $Ror\gamma t^+CD3^-$ ILC3s were counted and are shown. **i**, FFPE lung sections from 30 d.p.i. *Mtb*-infected mice were stained with antibodies against B220 and CD3, and the average size of B cell follicles was quantified. Significance is calculated by Student's *t*-test (**c**–**i**). Data are mean ± s.d. and individual values. All experiments were replicated at least twice.

nature research

Corresponding author(s): Shabaana Khader and Alasdair Leslie

Reporting Summary

Nature Research wishes to improve the reproducibility of the work that we publish. This form provides structure for consistency and transparency in reporting. For further information on Nature Research policies, see Authors & Referees and the Editorial Policy Checklist.

Statistical parameters

When statistical analyses are reported, confirm that the following items are present in the relevant location (e.g. figure legend, table legend, main text, or Methods section).

n/a	Confirmed	
☐	☒	The exact sample size (*n*) for each experimental group/condition, given as a discrete number and unit of measurement
☐	☒	An indication of whether measurements were taken from distinct samples or whether the same sample was measured repeatedly
☐	☒	The statistical test(s) used AND whether they are one- or two-sided *Only common tests should be described solely by name; describe more complex techniques in the Methods section.*
☒	☐	A description of all covariates tested
☐	☒	A description of any assumptions or corrections, such as tests of normality and adjustment for multiple comparisons
☐	☒	A full description of the statistics including central tendency (e.g. means) or other basic estimates (e.g. regression coefficient) AND variation (e.g. standard deviation) or associated estimates of uncertainty (e.g. confidence intervals)
☐	☒	For null hypothesis testing, the test statistic (e.g. *F*, *t*, *r*) with confidence intervals, effect sizes, degrees of freedom and *P* value noted *Give P values as exact values whenever suitable.*
☒	☐	For Bayesian analysis, information on the choice of priors and Markov chain Monte Carlo settings
☒	☐	For hierarchical and complex designs, identification of the appropriate level for tests and full reporting of outcomes
☒	☐	Estimates of effect sizes (e.g. Cohen's *d*, Pearson's *r*), indicating how they were calculated
☐	☒	Clearly defined error bars *State explicitly what error bars represent (e.g. SD, SE, CI)*

Our web collection on statistics for biologists may be useful.

Software and code

Policy information about availability of computer code

Data collection	Human clinical data captured using the Datafax system
Data analysis	Flow Cytometry data analyzed by FlowJo, Statistical analysis all conducted using GraphPad Prism.

For manuscripts utilizing custom algorithms or software that are central to the research but not yet described in published literature, software must be made available to editors/reviewers upon request. We strongly encourage code deposition in a community repository (e.g. GitHub). See the Nature Research guidelines for submitting code & software for further information.

Data

Policy information about availability of data

All manuscripts must include a data availability statement. This statement should provide the following information, where applicable:

- Accession codes, unique identifiers, or web links for publicly available datasets
- A list of figures that have associated raw data
- A description of any restrictions on data availability

Provide your data availability statement here.

Field-specific reporting

Please select the best fit for your research. If you are not sure, read the appropriate sections before making your selection.

☒ Life sciences ☐ Behavioural & social sciences ☐ Ecological, evolutionary & environmental sciences

For a reference copy of the document with all sections, see nature.com/authors/policies/ReportingSummary-flat.pdf

Life sciences study design

All studies must disclose on these points even when the disclosure is negative.

Sample size	No prior sample size calculations were performed for human studies. For the blood analysis, similar sample numbers were used as in previous studies reporting statistical differences between blood ILC populations (Kloverpris et al. Immunity 2015). For lung analysis, samples represent those collected over a 3 study period. For animal studies, sample sizes were chosen following empirical statistical power analysis based on previous pilot studies (Khader et al. 2007 Nat Immunol, Griffiths et al, 2016 etc).
Data exclusions	No human blood samples were excluded from analysis. Human lung samples were excluded if <10,000 viable CD45+ve leukocytes were detected by flow cytometry following sample processing. This was based on previous experience with lung tissue and was done prior to additional analysis steps. 6 lung sample in total were excluded on this basis.
Replication	For animal studies, all attempts at replication were successful.
Randomization	Human subjects divided into those with active TB, previous TB or non-TB controls as reported in the manuscript. For animal studies, no method of randomization was used.
Blinding	Blinding was not possible for human subjects due to the nature of sample collection and processing. For animal studies, J.R-M. was blinded during the histological analyses.

Reporting for specific materials, systems and methods

Materials & experimental systems

n/a	Involved in the study
☒	☐ Unique biological materials
☐	☒ Antibodies
☒	☐ Eukaryotic cell lines
☒	☐ Palaeontology
☐	☒ Animals and other organisms
☐	☒ Human research participants

Methods

n/a	Involved in the study
☒	☐ ChIP-seq
☐	☒ Flow cytometry
☒	☐ MRI-based neuroimaging

Antibodies

Antibodies used	All the antibodies used in human and mouse experiment is reported in methods in the "Flow cytometry" sections.
Validation	All antibodies commercially available flow cytometry antibodies for staining primary human or mouse samples and validated by the manufacturer. All antibodies titrated in house and compatibility with the flow panel confirmed by FMO staining.

Animals and other organisms

Policy information about studies involving animals; ARRIVE guidelines recommended for reporting animal research

Laboratory animals	The description of research animals used is reported in the methods in the "Mice" section.
Wild animals	*Provide details on animals observed in or captured in the field; report species, sex and age where possible. Describe how animals were caught and transported and what happened to captive animals after the study (if killed, explain why and describe method; if released, say where and when) OR state that the study did not involve wild animals.*

Field-collected samples	*For laboratory work with field-collected samples, describe all relevant parameters such as housing, maintenance, temperature, photoperiod and end-of-experiment protocol OR state that the study did not involve samples collected from the field.*

Human research participants

Policy information about studies involving human research participants

Population characteristics	For human PBMC samples - CUBS: n= 50; Median age 35 years (IQR 29-45); 66% female; 54% HIV infected; 80% on ARV at time of sampling; all drug susceptible TB infected subjects treatment naive at the time of sampling; all subjects with drug resistant TB on first line TB therapy at the time of sampling. FRESH: n=18; Median age 20 years (IQR 18-23); 100% female; all HIV negative by nucleic acid test; non-pregnant, non-anemic and with no signs and symptoms of chronic illness (reported in Dong et al, Lancet HIV 2017, https://doi.org/10.1016/S2352-3018(17)30146-7) For human TB lung samples n=30; Median age 39 years (IQR 31-61); 43% female; 57% HIV positive all on ART therapy, all subjects with previous TB on precautionary Rifafour TB treatment at the time of surgery. Treatment of active TB cases varied on a case by case basis depending on drug susceptibility and patient status. TB pathology confirmed by pathologist. Non-TB lung Samples n=5; Median 31 (IQR 24-55); 45% female, all HIV negative, negative TB status/cancer diagnosis confirmed by pathologist.
Recruitment	Human PBMC samples CUBS (TB infected): Participants are recruited from hospitals, primary health care clinics, HIV testing and counseling sites, HIV treatment clinics, universities and other relevant health care sites in KwaZulu Natal, South Africa. The relevant authorizations and approvals for each site was acquired before implementation of this protocol. Participants were identified by the research nurse based the eligibility criteria. The enrolling research team member then discussed the purpose of the study with the participant and they are asked to read and sign the consent form prior to recruitment. Clinical data was collected from participants and medical chart review. If HIV status is not known, participants may be referred for HIV counseling and testing. Participants who were on site were reimbursed R80 for participation. If the participants were required to travel to return for subsequent sample collection, they were reimbursed R150. FRESH (TB negative, HIV negative): Eligible women were HIV uninfected, aged 18-23 years, sexually active, not pregnant, non-anaemic, without other barriers to participation (serious chronic illness, enrollment in another study, or family responsibilities), and gave written consent to enrollment. More details of cohort can be found in Dong et al Lancet HIV 2017 (https://doi.org/10.1016/S2352-3018(17)30146-7) LUNG: Particpants are recruited from two sites based in Durban, South Africa; namely Inkosi Albert Luthuli Central Hospital (IALCH) and King Dinizulu Hospital Complex (KHDC). Collaborating surgeons identified individuals who are scheduled to have thoracocentesis and/or surgical procedures where lung tissue is excised. The enrolling research team member then contacted the potential participants to discuss the purpose of the study. This is conducted in the language that the participant is most comfortable with. The participant is asked to read and sign the consent form prior to recruitment. In the event that consent may not be acquired prior to the surgical procedure (e.g. emergency surgery), consent is obtained post-operatively. A copy of the informed consent document is given to the participants to keep. Participants are not reimbursed.

Flow Cytometry

Plots

Confirm that:

☐ The axis labels state the marker and fluorochrome used (e.g. CD4-FITC).

☒ The axis scales are clearly visible. Include numbers along axes only for bottom left plot of group (a 'group' is an analysis of identical markers).

☒ All plots are contour plots with outliers or pseudocolor plots.

☒ A numerical value for number of cells or percentage (with statistics) is provided.

Methodology

Sample preparation	Sample preparation is described in methods in the "Flow cytometry" section.
Instrument	Human cells were acquired on a 4 laser BD Fortessa flow cytometer (CUBS and FRESH blood samples) or a 5 laser FACSARIA Fusion (Lung, chemokine and apoptosis experiment samples) within 24 hours of processing. Mouse samples were acquired in Becton Dickinson (BD) Fortessa flow cytometer using FACS Diva software.
Software	All Human and mouse FACS data were analysed using FlowJo (TreeStar).
Cell population abundance	For sorting of human lung ILCs, a test lung sample was sorted and purity checked by re-acquiring sorted ILC population. Purity of

Cell population abundance	test sort was >95%. Subsequent sorts were not checked for purity due to low cell numbers, however, cell sorter (FACS ARIA) performance assessed before each sorting run using CST beads as per manufacturers instructions.
Gating strategy	For human flow cytometry experiments' singlets were gated based by plotting FSC-H vs FSC-A and then sub-gated on lymphocyte using FSC vs SSC characteristics. ILC populations were then identified using the antibody panels described in the text and in Extended figure 1. Positive gates where set using unstained control cells. For mouse experiments, gating strategy is reported in the text and also in the extended figure 3. Percentages of different cell types were gated based on both published strategies for APC cell types (Griffiths et al, 2016; Treerat et al, 2017) and ILC subsets gating is shown in Extended figure 3. Total cells per subset/lung were back calculated based on lung cell numbers.

☒ Tick this box to confirm that a figure exemplifying the gating strategy is provided in the Supplementary Information.